Arabian Journal of Geosciences (2022) 15:1582
https://doi.org/10.1007/s12517-022-10848-2

ORIGINAL PAPER

The provenance and history of Abu Muharak barchan sands (Kharga Depression) inferred from textural, mineralogical, and geochemical perspectives

Sayed Ramadan[1] · Mohamed A. Hamdan[1] · Ahmed M. Abu Khadra[1] · Mohamed Abdel Wahed[1]

Received: 2 May 2022 / Accepted: 17 September 2022 / Published online: 1 October 2022

Abstract
The current study deals with textural, mineralogical, and geochemical characteristics of the barchan dune sands of Abu Muharak dune belts in the Kharga Depression. Abu Muharak is the longest dune belt in the Western Desert of Egypt. Sand samples from 37 sites were texturally, petrologically, and chemically analyzed. Our goals were to interpret the provenance of the sands in terms of grain size, petrology, and geochemistry and correlate these data with the proposed source such as Nubian sandstone, Pleistocene alluvial, and Holocene lacustrine sediments as well as ancient aeolian deposits exposed at the Kharga Depression. The present study concludes that the Moghra sandstone is the main source of the Abu Muharak dune belt with local contributions from Pleistocene alluvial and dune deposits as well as weathered Nubian sandstone in the Kharga Depression.

Keywords Brachan · Petrology · Mineralogy · Geochemistry · Kharga Depression · Egyp

Introduction

The Abu Muharak dune belt is the most outstanding dune belt in the Western Desert of Egypt, attaining c. 800 km in length and 50 km in width, with various dune density and dune types, that extends from the Bahariya Depression in the north to the Egyptian Sudanese border in the south. Recently, Embabi (2017) ranked the Abu Muharak dune belt as the sand sea. The Abu Muharak dune belt is subdivided into three sectors; the northern and middle sectors consist mainly of linear dunes, whereas the southern section in the Kharga Depression consists mostly of barchan dunes (Hamdan et al. 2016).

Dunes in the Kharga Depression are mainly existing in the eastern and central parts of the depression and on the plateau to the north. They are assembled in discrete patterns extended in a north–south field and consist mainly of barchan dunes (Bagnold 1941; Gifford et al. 1979; Embabi 1982). Barchans are arranged into three parallel belts (western, central, and eastern belts), extending from north to south in a manner consistent with the direction of the prevailing winds. The western belt is the longest and largest within the Kharga Depression, with a total length and width attaining c. 195 km and 19 km, respectively. The central extends from the eastern end of the northwestern escarpment to the Kharga Oasis and begins in the form of an immobile linear dune, then turns into mobile barchans and several complex barchans and barchanoids. The eastern belt extends adjacent to the foot slope of the eastern escarpment of the depression for 25 km in the form of separate sand streaks. It seems that the three belts of the Kharga Depression are joined together in one sand sheet (c. 40 km in width) near the southern edge of the depression.

Several sources for the dune sand of Egypt have been considered in previous publications.

There are three main sources of sand in the Egyptian dune fields and sand seas: Upper Cretaceous Nubian sandstone (El-Baz 1988; El-Baz and Wolfe 1982) and Lower Miocene Moghra Formation in northern Egypt (Beadnell 1910; Ball 1927). The Nubian sandstone faced many arguments because it was exposed in southern Egypt, while the dunes migrate in an N-S direction parallel to the prevailing winds. The third source supposed that the aeolian sand of Egyptian deserts resumed its accumulation during

Responsible Editor: Attila Ciner

✉ Mohamed A. Hamdan
mhadan@cu.edu.eg

[1] Geology Department, Faculty of Science, Cairo University, Giza, Egypt

the last glacial maximum (LGM) when the sea level was lower by at least 120 m (Said 1998). The exposed continental shelf, which extends c. 40 km in the Mediterranean, was a reasonable source for the sands required to form the dune fields of the Western Desert of Egypt. This source is not fully accepted because the sediments at the exposed continental shelf are either calcareous sands or fine siliciclastic transported by the Nile River. Hamdan et al. (2015) used textural, mineralogical, and geochemical proxies to conclude that the formation of aeolian sand was a complex multicausal process formed in several alluvial, lacustrine, and aeolian environments throughout the Tertiary-Quaternary.

The current study investigates the variation and distribution of texture, mineralogy, and geochemistry of the sand of the barchan dunes in the Kharga Depression and aims to:

(1) Characterize the texture, mineral composition, and geochemistry of the sand in the Kharga Depression and the homogeneity of its composition throughout the dune field from the north to south direction.
(2) Study the textural and mineralogical variations of different parts of individual barchans.
(3) Determine the main sources of the sand of the Kharga dune field.
(4) Estimate the possible local contributions to the texture and composition of the Kharga sand from the exposed rocks and sediments in the pass of the moving barchans, i.e., carbonate grains.
(5) Compare the texture and composition of the sands of Kharga with the sand from another dune field in Egypt and worldwide.
(6) Contribute new data to enhance our knowledge about the history of the aeolian sand of the Egyptian deserts.

Geologic setting

The Kharga Oasis is the largest depression in the Western Desert of Egypt (Fig. 1A). It extends from north to south for 160 km along the western edge of the Egyptian plateau. It is bounded from the west by dune belts and from the north and east by huge escarpments. The geology of the Kharga Depression is represented by the Upper Cretaceous-Lower Tertiary sedimentary sequence that overlies unconformably the Precambrian basement rocks (Fig. 1B). This sedimentary sequence consists of three lithological units; (1) the lower clastic succession which is represented from older to younger by the Nubian sandstone, Quseir variegated shale, Dawi phosphate, and Dakhla shale; (2) the middle unit which is represented by the Paleocene Tarawan chalk and Esna Shale; (3) the upper unit is represented by lower Eocene Thebes Limestone (Fig. 1B).

Nubian sandstone is exposed at the central and southern part of the Kharga Depression and extends to the foot-slope of the escarpments of the depression. It attains a thickness of c. 200 m of a highly dissected, cross-bedded coarse- and fine-grained sandstone. This unit is composed entirely of quartz arenite with trace amounts of feldspar and rock fragments with minor amounts of arkosic (subarkosic) arenite and litharenite (or sublitharenite).

Quseir variegated shale is found in multiple colors, including red, green, gray, and brown, and often contains plant remains and vertebrate fossils. Dawi phosphate is exposed in the northern part of the depression consisting of several phosphate beds c. 2–3 m in thickness. Dakhla shale, which overlies phosphate beds of Kharga, and consists of clay, gray gypsum veinlets, and limestone, extends on the eastern edge of the Kharga depression, with a maximum thickness of 100 m (Said 1962). The Tarawan and Esna formations of the Paleocene rocks cover most parts of the northern and the eastern escarpments of the Kharga depression and are represented by two lithologies; the first consists of c. 85-m-thick fossiliferous limestone intercalated with thin shale and sandstone layers. The second lithology consists of white chalky limestone with shale interbeds, 50 to 120 m in thickness. Lower Eocene rocks are represented in the Thebes Formation (limestone with marl interbeds) and cover the top of the plateau overlooking the Kharga Depression.

Quaternary sediments are represented by spring deposits (tufa), alluvial deposits, lacustrine (playa) sediments, and dunes. Tufa is composed of porous carbonate rock masses, very rough, with a pale-yellow color that turns black on the exposed surfaces. Alluvial sand and gravel terraces exist in the form of horizontal terraces of different heights, at the foot-slope of the northern and eastern escarpments. Lacustrine (playa) sediments are horizontal deposits of silt and fine sand with a thickness of several meters. It seems that most of the Quaternary along with the clastic units of the Kharga Depression could be a suitable sand feeder to the dune sands.

Materials and methods of study

Fifty-four barchan sand samples were collected from the Kharga dune fields (Fig. 2A). In each dune, seven samples were collected from the crest, windward, base, mid-slip, right and left horns as well as the interdunal area (Fig. 2B). Approximately 100 g of sample was used for grain size analysis. Textural parameters like graphic mean size (Mz); inclusive graphic sorting (σ_1); inclusive graphic skewness (Sk_1); and kurtosis (KG) (Folk 1978) was determined using a dry sieving technique (Table 1). The roundness and sphericity of quartz grains of the aeolian dune sands of the Kharga Depression area were examined in 21 samples (Tables 2 and 3). The medium sand (1–2 Φ) and fine sand (2–3 Φ) fractions for each sample were examined using a digital microscope. About 100 grains were examined and described using the terminology

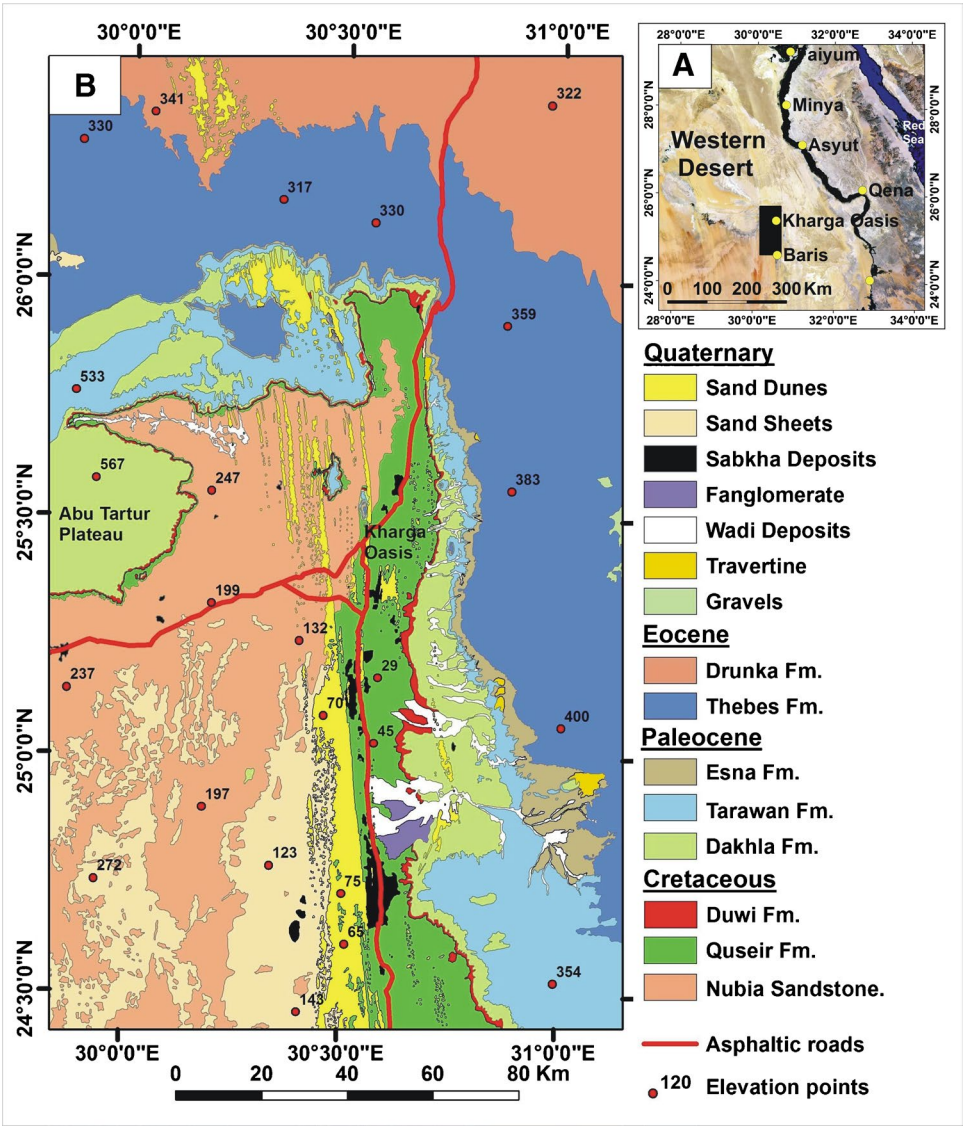

Fig. 1 **A** Location of the Kharga Depression. **B** Geologic map of the Kharga Depression, modified after Conoco Coral (1987)

proposed by Powers 1953 and adapted to a logarithmic ρ scale (Folk 1955). Quartz grains were classified and counted as VA, very angular; A, angular; SA, subangular; SR, subrounded; R, rounded; and VR, very rounded (Table 2). Then, roundness ratios VA/A (very angular/angular), SA/SR (subangular/ subrounded), and R/VR (rounded/very rounded) were determined to be used as poles in a ternary diagram. To study the surface features of quartz grains, 12 samples of barchan were examined by scanning electron microscope (SEM). The light and heavy minerals were separated from the fine sand fractions of 31 samples (Table 4). Separation was conducted using bromoform (density 2.85 at 20 °C; Milner 1962) in samples of fine sand size $^{>}$ 125 µm. Light and heavy fractions were washed with alcohol, dried, weighed and their percentages were calculated. The separated fractions were examined microscopically and the relative proportions of the various light- and heavy-mineral species were determined and cited in Tables 4 and 5.

X-ray fluorescence (XRF) was used to determine the major and trace element composition for 10 samples representing different dune types. Representative sediments subsamples are initially wet sieved to remove silt and clay-sized materials and dry sieved to remove grains coarser than -0.25 Φ in size. The subsamples were ground to produce a crushed powder and then mixed with lithium tetraborate to prepare fusion discs with a sample to flux ratio of 1:4. Major elements' concentrations (Tables 6) were determined.

Results and discussion

Color of the sand of the Kharga barchan

The color of Kharga barchan sands is measured by using the Munsell color chart. The sands are mostly yellow (10YR8/6)

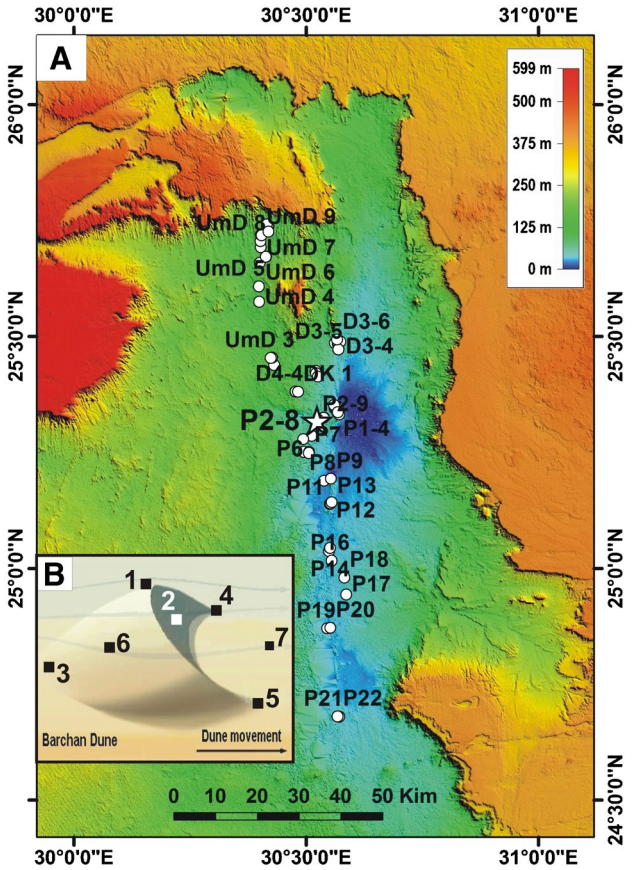

Fig. 2 **A** Shaded relief model of Kharga Depression showing the main geomorphic units and location of the studied barchan dune samples. **B** Location of samples in individual banchan, 1—crest, 2—mid-slip, 3—base, 4—left horn, 5—right horn, 6—windward, and 7—interdune

in color. Some dune sands show lighter pale yellow (2.5YR8.4) color or a little darker pinkish-gray (5YR6/2). The color variation is attributed to contribution from local sources, i.e., Upper Cretaceous chalk and shale from Quseir formations, respectively. The color of the Cretaceous bedrock in the Kharga Depression is changing from one rock unit to another; Nubian sandstone is light in color with 10 YR, while Quseir is reddish with 7.5YR (Besler 2008). The eroded aeolianite of the Quseir Formation could have provided reddish sands that should not have been transported too far. The color of the Kharga barchan sands is much lighter than those of the sand of the Great Sand Sea, which are much reddish (7.5 YR) and even red (5 YR) hues (Besler 2008), and lighter than those of the northern Western Desert (El-Baz et al. 1979). The reddish colors of quartz sands are caused by iron oxides associated with clay coatings. A thin-section analysis revealed multiple layers of clay stained with iron oxides (Besler 1998). Sand grains of southwestern Egypt with a reddish-brown coating that contains crystallized kaolinite and little hematite content (El-Baz et al. 1979).

Textural characteristics

Grain size distribution

Grain size distribution in the barchan sands of Kharga Depression is characterized by a unimodal pattern with the modal class of 250–125 mμ (i.e., medium to fine-grained sand size). Figure 3 shows the distribution curves of sand samples taken from various parts of three barchans representing the northern, central, and southern parts of the Kharga dune belt. There is a slight variation in the grain size distribution of sand from different parts of the Kharga barchans. Samples UMD11-1 and D3-6 at the northern and central parts of the dune field show that all parts of the barchan dune exhibit unimodal patterns with a slight variation in the values of the modal classes. There is little shifting toward finer modal class from the crest to windward samples and an almost similar pattern on the two horns (Fig. 3A). On the sample of the central part of the Kharga dune field, only one pattern most likely exists except for two samples of windward and the left horn (Fig. 3B). The grain size distribution on the southern part of the Kharga dune field (sample P22) shows a bimodal pattern on the samples of different dune parts (Fig. 3C). On all samples, interdunal sediments are much coarser and show a polymodal pattern (Fig. 3).

Graphic mean size

The graphic mean size (Mz) of all studied sand samples varies between 1.61 to 2.51 Φ with an average value of the mean size of 2.09 (Table 1). The sand in the southern part of the Kharga dune field is a little coarser with a mean size of 1.78 Φ, while the sand of the northern and central parts of the dune field is similar to the mean size of all samples (Table 1). There is a slight variation in the average values of the mean size in various parts of the Kharga barchan dunes (see Table 1). The crest and mid-slip samples of the studied barchan are the finest, and the base and windward samples are slightly coarse (Table 1). The samples of the interdune are much coarser than the barchan sand samples.

Inclusive graphic sorting

The values of the inclusive graphic sorting (σ_1) of the studied aeolian sands vary between 0.17 Φ (very well sorted) to 1.13 Φ (poorly sorted) with an average value of 0.78 Φ (moderately well sorted), which is worse sorted than the world average value (0.53 Φ; Goudie et al. 1987). There is a little variation in the sorting values of the sands of different parts of the Kharga dune field and within the individual dunes (Table 1). The sands of the barchan dunes of the northern part of the Kharga dune field exhibit better average sorting values than the central and southern parts (Table 1). The average sorting values of the barchan sands systematically vary from one part to another of

Table 1 Grain size parameters of the Kharga barchan sands

Sample location	Sector	Median	Range	Mean	Range	Sorting	Range	Skewness	Range	Kurtosis	Range
Crest ($n=25$)	Northern	2.02	2.35–1.59	1.99	2.42–1.56	0.75	1.11–0.13	0.28	0.81–0.10	1.04	− 1.28–1.88
	Central	1.82	2.51–1.07	1.78	2.51–0.96	0.17	0.33–0.97	1.02	1.46–0.74	1.02	0.74–1.46
	Southern	1.87	2.12–1.7	1.87	2.12–1.70	1.00	1.58–0.64	0.36	0.57–0.01	1.25	0.74–1.54
	Average	1.90	2.33–1.45	1.88	2.35–1.41	0.64	1.00–0.58	0.55	0.94–0.27	1.11	0.07–1.63
Mid slip ($N=25$)	Northern	2.18	2.47–1.66	2.21	2.47–1.61	0.84	0.93–0.68	0.10	0.15–0.03	1.46	0.87–1.91
	Central	2.26	2.55–2.05	2.33	2.55–2.13	0.75	0.97–0.56	− 0.01	0.29–0.17	1.18	1.02–1.46
	Southern	2.25	2.63–1.91	2.19	2.43–1.85	0.97	0.4–1.42	0.22	0.42–0.10	1.38	0.76–1.93
	Average	2.23	2.55–1.87	2.25	2.48–1.87	0.85	1.11–0.62	0.10	− 0.02–0.29	1.34	0.89–1.77
Base ($n=25$)	Northern	2.06	2.23–1.69	2.09	2.31–1.63	0.12	0.94–3.60	0.06	− 0.23–0.61	− 0.70	− 11.08–1.32
	Central	1.64	2.50–0.57	1.68	2.50–0.57	0.56	0.76–0.34	− 0.05	− 0.22–0.17	0.91	0.74–1.18
	Southern	2.26	3.26–1.73	2.14	2.83–1.65	0.96	1.41–0.55	0.22	− 0.01–0.40	1.21	0.74–2.02
	Average	1.99	2.66–1.33	1.97	2.55–1.28	0.54	1.03–0.90	0.08	− 0.15–0.39	0.47	− 3.20–1.51
LH ($n=25$)	Northern	2.14	2.54–1.73	2.13	2.51–1.65	0.79	0.99–0.56	0.15	0.01–0.28	1.40	0.83–2.13
	Central	2.19	2.76–1.22	2.18	2.57–1.15	0.91	1.24–0.45	0.07	− 0.16–0.39	1.44	0.88–2.17
	Southern	2.26	2.95–1.92	2.17	2.63–1.82	0.99	1.55–0.69	0.25	0.04–0.50	1.31	0.88–2.05
	Average	2.20	2.75–1.62	2.16	2.57–1.54	0.89	1.26–0.57	0.16	− 0.04–0.39	1.39	0.86–2.12
RH ($n=25$)	Northern	2.39	4.10–1.95	2.13	2.37–1.89	0.50	1.03–0.91	0.03	− 0.16–0.26	0.94	0.33–1.67
	Central	2.18	2.70–1.62	2.17	2.58–1.68	0.85	1.24–0.58	0.06	0.25–0.40	1.22	0.74–2.15
	Southern	2.22	2.87–1.75	2.15	2.57–1. 72	1.03	1.28–0.85	0.25	0.10–0.39	1.40	1.23–1.75
	Average	2.26	3.23–1.78	2.15	2.51–1.76	0.79	1.18–0.17	0.11	− 0.10–0.35	1.18	0.77–1.86
WW ($n=25$)	Northern	2.47	3.07–2.15	2.38	2.66–2.15	1.06	1.27–0.94	0.25	0.12–0.42	1.42	1.15–1.69
	Central	2.01	2.53–1.52	1.96	2.53–1.48	0.83	1.12–0.46	0.19	0.08–0.29	1.14	0.89–1.39
	Southern	2.22	2.87–1.75	2.15	2.57–1.72	1.03	1.28–0.85	0.25	0.10–0.39	1.40	1.23–1.75
	Average	2.23	2.82–1.81	2.16	2.59–1.78	0.97	1.22–0.75	0.23	0.10–0.37	1.32	1.09–1.61
Average barchan ($n=150$)		2.14	2.72–1.64	2.09	2.51–1.61	0.78	1.13–0.30	0.21	0.01–0.45	1.13	0.08–1.75
Inter-dune ($n=20$)	Northern	0.85	1.47–0.18	0.38	1.34–0.56	2.14	2.28–1.96	0.38	0.13–0.70	0.80	0.75–0.85
	Central	0.85	1.50–0.16	0.28	1.21–0.51	2.24	2.38–1.98	0.50	0.14–0.70	0.72	0.73–0.84
	Southern	0.86	1.58–0.14	0.08	1.44–0.61	2.2	2.64–2	0.52	0.18–0.72	0.74	0.7–0.77
	Average	0.85	1.52–0.16	0.25	1.33–0.56	2.20	2.43–1.98	0.47	0.15–0.70	0.75	0.73–0.82
Average all samples (n = 170)		1.96	2.56–1.44	1.84	2.34–1.31	0.98	1.31–0.53	0.24	0.03–0.49	1.08	0.17–1.62

Table 2 The roundness of the Kharga barchan sands

Sample no	Latitude	Longitude	VR % 6–5	R % 5–4	SR % 4–3	SA % 3–2	A % 2–1	VA % 0–1	VA/A	SA/SR	R/VR	ρ
UMD12	25° 44′ 29″.7	30° 24′ 56″.4	9.17	30.64	37.52	14.4	4.59	3.67	0.8	0.38	3.34	3.6
UMD11-1	25° 44′ 13″	30° 25′ 11″.3	12.56	34.88	30.23	16.28	4.65	1.4	0.3	0.54	2.78	3.7
UMD13	25° 43′ 34″	30° 25′ 08″.9	10.29	32.63	32.92	16.69	4.58	2.88	0.44	0.51	3.17	3.75
UMD10-1	25° 43′ 06″.1	30° 24′ 15″.4	10.89	34.65	29.7	18.8	4.47	1.49	0.43	0.63	3.18	3.7
UMD15	25° 40′ 19″.28	30° 24′ 49″.31	10.89	34.65	29.7	18.8	4.47	1.49	0.43	0.63	3.18	3.6
UMD16	25° 40′ 18″.4	30° 24′ 47″.5	7.44	34.88	36.16	14.53	4.65	2.33	0.5	0.4	4.69	3.5
D3-4	25° 29′ 20″.1	30° 34′ 25″.0	6.77	35.28	35.3	15.09	5.66	1.89	0.33	0.43	5.21	3.6
D3-3	25° 29′ 13″.1	30° 34′ 07″.2	7.34	28.35	32.11	22.11	6.88	3.21	0.47	0.69	3.86	3.5
P3-1	25° 29′ 05″.1	30° 34′ 05″.6	6	26	33	25	8	2	0.5	0.76	4.33	3.4
UMD17	25° 28′ 36″.9	30° 24′ 36″.4	5.66	26.43	31.53	27.85	9.75	2.77	0.18	0.88	4.67	3.3
D3-6	25° 28′ 18″.8	30° 34′ 10″.4	5.71	28.57	30	25.14	9.43	1.14	0.15	0.84	5	3.5
D4-2	25° 25′ 13″	30° 31′ 17″	3.77	25.28	38.3	25.09	5.66	1.89	0.33	0.66	6.7	3.2
P1-4	25° 20′ 13″.1	30° 34′ 06″.4	3.19	20.36	28.34	39.19	6.07	2.83	0.47	1.38	6.38	3
P2-8	25° 19′ 05″.9	30° 31′ 24″.9	3.31	20.54	32.31	36.51	5.02	2.32	0.46	1.13	6.21	2.8
P2-8 Horn	25° 19′ 05″.9	30° 31′ 24″.9	6.12	19	37.82	28.53	6.12	2.44	0.4	0.75	3.1	3.3
P2-8 Crest	25° 19′ 05″.9	30° 31′ 24″.9	8.89	20.89	40	23.56	4.44	2.22	0.5	0.59	2.35	3.5
P2-8 base	25° 19′ 05″.9	30° 31′ 24″.9	9.31	16.54	30.31	36.51	5.02	2.32	0.46	1.2	1.78	2.8
P2-8 MS	25° 19′ 05″.9	30° 31′ 24″.9	7.24	24.48	27.86	33.09	4.74	2.59	0.55	1.19	3.38	2.9
P4-2	25° 16′ 42″.3	30° 29′ 37″.5	2.89	18.89	26	35.56	14.44	2.22	0.5	1.37	6.54	2.6
P7	25° 14′ 55″.7	30° 30′ 21″.8	2.28	13.7	29.68	36.53	13.7	4.11	0.3	1.23	6	2.5
P11	25° 08′ 18″.2	30° 33′ 05″.0	2.12	18.37	34.82	36.53	6.12	2.04	0.33	1.05	8.65	2.7
P16B	25° 01′ 00″.3	30° 33′ 18″.8	2.44	14.88	36.16	39.53	4.65	2.33	0.5	1.09	6.09	2.6
P19	24° 52′ 14″.1	30° 32′ 43″.8	2.28	11.7	31.68	36.53	13.7	4.11	0.3	1.15	5.12	2.7
P22	24° 40′ 51″.5	30° 34′ 04″.8	1.58	10.04	34.33	36.31	15.58	2.15	0.38	1.06	6.34	2.8
Average			6.17	24.23	32.74	27.42	7.18	2.41	0.42	0.86	4.67	3.19
MaxU+F073).			12.56	35.28	40	39.53	15.58	4.11	0.8	1.38	8.65	3.75
Min			1.58	10.04	26	14.4	4.44	1.14	0.15	0.38	1.78	2.5

VA, very angular; *A*, angular; *SA*, subangular; *SR*, subrounded; *R*, rounded; *VR*, very rounded

the same dune: for example, base and crest, and samples the better average sorted values of 0.54 *Φ* and 0.62 *Φ*, respectively. Windward and mid-slip samples show poorly sorting values that averaging 0.97 and 0.85 *Φ*, respectively. The sand of horns of the barchan dunes exhibits moderately sorting with an average sorting value of about 0.79 *Φ*. The samples of the interdune sands are the worse sorted values of all studied barchan samples which attains c. 2.2 *Φ* (Table 1).

Inclusive graphic skewness

Most of the studied dune sands are positively fine skewed to nearly symmetric (e.g., Mason and Folk 1958; Pye 1982). Indeed, the presence of a suspension population and the truncation of the coarse population account for the positive skewness characteristic of dune deposits (Visher 1969). The average measured skewness value of all samples is about 0.21 (nearly symmetric). They range between 0.01 (nearly symmetric) for linear and 0.45 (fine skewed). There is little variation in the average skewness values from different parts of the studied barchan dunes (Table 1). For example, the crests of the studied barchan sands show an average skewness value of 0.55 (nearly symmetric) and vary from 0.27 (fine skewed) to 0.94 (moderately symmetric). This is probably attributed to the selective removal of finer particles from the dune crest by the wind. The average skewness values of the other barchan parts are markedly low (i.e., nearly symmetric), but with a very narrow range from 0.08 to 0.23 (see Table 1). The samples of the interdune are varied in average skewness values from 0.15 to 0.7 with an average value of 0.47 (Table 1). There is also little increase in the measured skewness values of the barchan sand from the northern, central, and southern parts of the depression, respectively (Table 1).

Kurtosis

The kurtosis values (KG) of most barchan sands in the Kharga Depression are mesokurtic and platykurtic to very platykurtic, with an average of 1.13 (ranging from 0.08 to

Table 3 The sphericity of Kharga barchan sands

Samples	Latitude	Longitude	P. spherical	M. spherical	spherical	W. spherical	ρ
Um 11–1	25° 44′ 13″ N	30° 25′ 11″.3 E	6.85	27.40	54.79	10.96	2.50
Um 13 MS	25° 43′ 34″ N	30° 25′ 08″.9 E	11.90	26.19	47.62	14.29	2.50
Um 15 WW	25° 40′ 19″.28 N	30° 24′ 49″.31 E	4.55	22.73	53.03	19.70	2.60
Um 15 B	25° 40′ 19″.28 N	30° 24′ 49″.31 E	8.97	28.21	47.44	15.38	2.50
Um 16 WW	25° 40′ 18″.4 N	30° 24′ 47″.5 E	9.09	23.64	45.45	21.82	2.50
D3-3	25° 29′ 13″.1 N	30° 34′ 07″.2 E	3.85	35.90	50.00	10.26	2.30
D3-4	25° 29′ 20″.1 N	30° 34′ 25″.0 E	7.25	32.07	50.72	9.96	2.20
D3-5	25° 29′ 18″.8 N	30° 34′ 10″.4 E	3.94	39.39	47.58	9.09	2.10
Um 17	25° 28′ 36″.9 N	30° 24′ 36″.4 E	7.41	28.89	48.89	14.81	2.40
Um 2 LW	25° 27′ 14″.6 N	30° 25′ 36″.1 E	4.17	20.83	61.11	13.89	2.70
P1-14 crest	25° 21′ 7″.4 N	30° 33′ 36″.8 E	5.56	20.83	55.56	18.06	2.60
P2-8 base	25° 19′ 05″.9 N	30° 31′ 24″.9 E	10.20	20.41	61.22	8.16	2.70
p2-8 LH	25° 19′ 05″.9 N	30° 31′ 24″.9 E	15.38	23.08	46.15	15.38	2.20
P2-8 MS	25° 19′ 05″.9 N	30° 31′ 24″.9 E	7.94	15.87	63.49	12.70	2.70
P2-8 RH	25° 19′ 05″.9 N	30° 31′ 24″.9 E	6.25	18.75	62.50	12.50	2.60
P3-1	25° 17′ 7″.7 N	30° 30′ 44″.8 E	4.76	23.81	55.56	15.87	2.60
P9	25° 11′ 35″.8 N	30° 33′ 13″.1 E	6.10	24.39	48.78	20.73	2.30
P15 b	25° 02′ 39″.4 N	30° 33′ 07″.2 E	7.69	30.77	46.15	15.38	2.40
P17	24° 56″ 36″.3 N	30° 35′ 10″.9 E	11.90	23.81	47.62	16.67	2.40
P22	24° 40′ 51″.5 N	30° 34′ 04″.8 E	5.41	27.03	54.05	13.51	2.70
P21	24° 40′ 48″.8 N	30° 34′ 15″.2 E	6.56	26.23	54.10	13.11	2.70
Average			7.42	25.72	52.47	14.39	2.49
Max			15.38	39.39	63.49	21.82	2.70
Min			3.85	15.87	45.45	8.16	2.10

1.75). there is no significant spatial variational trend that exists in the kurtosis of grain size between the northern, central, and southern parts of the Kharga dune belt (Table 1).

Bi-variant interrelation of the grain size parameters

Little variation in grain size parameters has been found since the winds can transport only a narrow size range by saltation or other modes of transport (Bagnold 1941). Generally, the grain size properties of aeolian barchan sands are functions of the source material, selective wind transportation, and the topography of the initial surface. Figure 4A is a scatter plot diagram of the mean size (Mz) versus standard deviation (σ_1). It shows that the best sorting values are attained by medium to fine sands at a mean size of 0.5 Φ and 1.5 Φ. Sorting becomes worse as the sand gets either finer or coarser, which agrees with the conclusion reached by Folk and Ward (1957). There is a poor correlation between the mean size and sorting of the sands of the different parts of the barchan dunes. The values of R^2 range from 0.0002 (windward samples to 0.14442 (base samples). Such poor correlation between the mean size and sorting could be attributed to the direct supply of sand from local sources, i.e., weathered Nubian sandstone alluvial and playa sediments, especially in the middle and southern part of the Kharga dune field.

The bivariant diagram of the mean size versus skewness (Fig. 4B), shows a very poor correlation (R^2 ranging between 0.0001in base samples to 0.108 in crest samples). It also shows that, as the mean size decreases the more positive skewness will result and are plotted together as a mixed group. Most of the studied dune sand is nearly symmetrical to positive skewed, and few samples are negatively skewed which are likely related to the northern part of the dune field. There is a strong correlation between the mean size versus kurtosis of the studied samples (Fig. 4C); the best correlation was found on the samples of the crest, mid-slip, and the two horns while the worse relation is found on the base and windward as well as the interdune samples. There is a general tendency for the kurtosis to change to platy-kurtic and very platy-kurtic, as the size decreases. There is also a strong correlation between the sorting and the skewness of the studied aeolian sand samples (Fig. 4D).

Comparison of the sand of the Kharga barchans with other barchan sands

In comparison, the grain size parameter of the Kharga dune field is a little finer than the Toshka sand (Hamdan et al. 2015) but coarser than the Abu Muharak sand (Embabi

Table 4 Light minerals of Kharga barchan sands

Sample	Latitude	Longitude	MS	MU	MI	MQ	PQ	Total Q	KF	Pl	Total F	RF
UMD12 (MS)	25° 44′ 29″.7 N	30° 24′ 56″.4E	63.6	14.5	3.6	81.8	9.1	90.9	3.6	2.7	6.4	2.7
UMD12 (L. Horn)	25° 44′ 29″.7 N	30° 24′ 56″.4E	61.8	13.6	4.5	80	8.2	88.2	5.5	3.6	9.1	1.6
UMD11-1 (Crest)	25° 44′ 13″N	30° 25′ 11″.3E	49.7	15.5	4.7	69.8	9.3	79.1	5.4	3.9	9.3	13.1
UMD13 (WW)	25° 43′ 34″N	30° 25′ 08″.9E	33.8	13.1	6.2	73.1	13.1	66.2	6.2	4.6	10.8	32.6
UMD13 (L. Horn)	25° 43′ 34″N	30° 25′ 08″.9E	52.6	13.8	6.6	73	14.5	87.5	5.3	4.6	9.9	3.8
UMD10-1 (Base)	25° 43′ 06″.1 N	30° 24′ 15″.4E	56.8	12.1	3.8	72.7	12.1	84.8	6.1	5.3	11.4	3.8
UMD10-2 (Crest)	25° 43′ 06″.1 N	30° 24′ 15″.4E	51	14	7	72	14.6	86.6	5.7	3.8	9.6	4.5
UMD15 (MS)	25° 40′ 19″.28 N	30° 24′ 49″.31E	54.5	12.9	7.6	75	11.4	86.4	5.3	3.8	9.1	3.2
UMD16 (Crest)	25° 40′ 18″.4 N	30° 24′ 47″.5E	51.1	10.3	6.3	67.8	10.3	78.1	6.3	2.4	8.7	12.9
D3-4 (R. Horn)	25° 29′ 20″.1 N	30° 34′ 25″.0E	58.1	11	8.8	77.9	10.3	88.2	5.1	3.7	8.8	3.6
D3-3 (L. Horn)	25° 29′ 13″.1 N	30° 34′ 07″.2E	56.1	10.1	9.4	75.5	10.8	86.3	5.8	4.3	10.1	3.1
P3-1 (WW)	25° 29′ 05″.1 N	30° 34′ 05″.6E	60.2	10.9	7	78.1	9.4	87.5	5.5	3.9	9.4	3.2
UMD17 (MS)	25° 28′ 36″.9 N	30° 24′ 36".4E	51.9	13	7.1	72.1	14.3	86.4	6.5	3.9	10.4	18.7
UMD17 (WW)	25° 28′ 36".9 N	30° 24′ 36".4E	48.2	8.4	7.5	64.1	13.4	92.5	0	3.7	3.7	2.9
D3-6 (L. Horn)	25° 28′ 18".8 N	30° 34′ 10".4E	58.1	11	8.8	77.9	10.3	88.2	5.1	3.7	8.8	3.8
D4-2 (MS)	25° 25′ 13"N	30° 31′ 17″ E	50.3	13.8	6.9	71.1	14.5	85.5	6.9	3.8	10.7	2.7
P1-4 (Crest)	25° 20′ 13".1 N	30° 34′ 06".4E	54.4	13.4	8.1	75.8	13.4	89.3	4.7	3.4	8.1	2.9
P1-4 WW	25° 20′ 13".1 N	30° 34′ 06".4E	58.1	11	8.8	77.9	10.3	88.2	5.1	3.7	8.8	3.8
P2-8 (R. Horn)	25° 19′ 05".9 N	30° 31′ 24".9E	56.8	10.8	7.9	75.5	12.9	88.5	5.8	3.6	9.4	2.5
P2-8 (L. Horn)	25° 19′ 05".9 N	30° 31′ 24".9E	57.4	10.3	9.6	77.2	12.5	89.7	5.1	2.9	8.1	2.2
P2-8 (Crest)	25° 19′ 05".9 N	30° 31′ 24".9E	51.3	14.1	7.1	72.4	14.7	87.2	5.1	3.8	9	3.5
P2-8 (Base)	25° 19′ 05".9 N	30° 31′ 24".9E	57.7	10.9	8.8	77.4	10.2	87.6	5.8	3.6	9.5	3.5
P2-8 (MS)	25°19′ 05".9 N	30° 31′ 24".9E	55.3	13.5	7.8	76.6	12.1	88.7	4.3	3.5	7.8	2.6
P2-8 (WW)	25° 19′ 05".9 N	30° 31′ 24".9E	53	13.9	7.9	74.8	13.9	88.7	5.3	3.3	8.6	2.2
P2-8 (Interdune)	25° 19′ 05".9 N	30° 31′ 24".9E	55.3	12.8	7.1	75.2	12.8	87.9	5	3.5	8.5	2.9
P4-2 (MS)	25° 16′ 42".3 N	30° 29′ 37".5E	65	12.5	4.2	81.7	7.5	89.2	5	3.3	8.3	3
P7 (Interdune)	25° 14′ 55".7 N	30° 30′ 21".8E	54.5	12.9	6.1	73.5	12.9	86.4	6.1	4.5	10.6	2.6
P11 (Base)	25° 08′ 18".2 N	30° 33′ 05".0E	65.5	13.8	3.4	82.8	8.6	91.4	3.4	2.6	6	2.6
P16B (L. Horn)	25° 01′ 00".3 N	30° 33′ 18".8E	42.3	14.4	7.2	63.9	15	78.9	5.2	3.3	8.5	13.8
P19 (WW)	24° 52′ 14".1 N	30° 32′ 43".8E	56.8	12.1	3.8	72.7	12.1	84.8	6.1	5.3	11.4	3.9
P22 (Base)	24° 40′ 51".5 N	30° 34′ 04".8E	51.9	14.3	7.1	73.4	14.9	88.3	3.9	3.9	7.8	3.9
Average			54.62	12.54	6.80	74.60	11.92	86.36	5.17	3.74	8.92	5.55
Max			65.5	15.5	9.6	82.8	15	92.5	6.9	5.3	11.4	32.6
Min			33.8	8.4	3.4	63.9	7.5	66.2	0	2.4	3.7	1.6

et al. 2012). The measured mean size values of the studied barchan sand are close to those of the Toshka barchans (1.2 *Φ*; Hamdan et al. 2015) and slightly coarser than the barchan dune sands of the Dakhla Oases (2.19 *Φ*; Sharaky 1990). This value is nearly like the average mean size of linear dunes in the northwestern Desert of Egypt (1.75 *Φ*; Hamdan and Refaat 1999), and is finer than the average mean size of the sands at the Great Sand Sea (Hamdan 2003). It seems that the mean size values of Kharga sands are comparable with the world average (2.23 *Φ*) mean grain size of most of the aeolian dune sand (Goudie et al. 1987). Figure 5 shows the relationship between mean size and sorting of aeolian sands from Egypt and worldwide deserts. The studied sands are plotted close to those of other Egyptian barchans, e.g., Toshka, SW Egypt, and the north Abu Muharak dunes (Hamdan et al. 2015; Maxwell 1982; Embabi et al. 2012). The studied aeolian sands are finer than those of Australia and Oman (Goudie et al. 1987) and worse sorting than those of Namib, Texas, and the Skelton coast (Mason and Folk 1958; Lancaster 1981). This may be due to the abundance of coarse sands produced by the disintegration of coarse-grained sandstone beds in the Kharga Depression and the Toshka desert. The average mean size of the studied linear dune sand is like the Gilf-Uwinat area (Hamdan 2003) as well as those in other deserts: the Libyan Desert (Bagnold 1941) and southwestern Libya, and the Namib Desert (Lancaster 1995). The grain size analysis indicates a fining up in mean size from the inter-dune and base samples to the crest

Table 5 Heavy minerals of Kharga barchan sands

Sample	Coordinate	ZR	TO	RU	ST	GA	And	EP	AM	PX	MI	S	ME	U	S/U	GA/EP
UMD12 LH	25° 44′ 29″.7 N/30° 24′ 56".4E	35.1	7	7	8.8	8.8	7	5.3	1.8	1.8	17.5	49.1	24.6	8.8	5.58	1.66
UMD12 LEFT	25° 44′ 29″.7 N/30° 24′ 56″.4E	11.8	19.7	15.7	15.7	14.2	4.7	6.3	1.6	0.8	9.4	47.2	34.6	8.7	5.43	2.25
UMD11-1	25° 44′ 13″ N/30° 25′ 11″.3E	30.4	10.4	8.7	10.4	13.9	8.7	6.1	1.7	0.9	8.7	49.6	33	8.7	5.70	2.28
UMD13 LEFT	25° 43′ 34″ N/30° 25′ 08″.9E	23.2	19.7	8.5	16.9	9.2	5.6	6.3	2.1	1.4	7	51.4	31.7	9.9	5.19	1.46
UMD13 WW	25° 43′ 34″ N/30° 25′ 08″.9E	29.6	18.5	7.4	7.4	15.7	4.6	4.6	1.9	0.9	9.3	55.6	27.8	7.4	7.51	3.41
UMD10-1	25° 43′ 06″.1 N/30° 24′ 15″.4E	26.9	22.4	11.2	7.5	11.2	5.2	4.5	2.2	1.5	7.5	60.4	23.9	8.2	7.37	2.49
UMD10-2	25° 43′ 06″.1 N/30° 24′ 15″.4E	24.2	18.2	6.1	18.2	12.1	8.5	6.7	1.2	1.2	3.6	48.5	38.8	9.1	5.33	1.81
UMD15 MS	25° 40′ 19″.3 N/30° 24′ 49″.3E	23.3	20	10.7	16	12	6	4	0.7	0.7	6.7	54	24	15.3	3.53	3.00
UMD16 Cr	25° 40′ 18″.4 N/30° 24′ 47″.5E	40	16.4	9.1	5.5	7.3	5.5	5.5	0.9	0.9	9.1	60.5	18.2	12.3	4.92	1.33
D3-4 RIGHT	25° 29′ 20″.1 N/30° 34′ 25″.0E	23.4	14.9	11.7	10.6	14.9	7.4	4.3	1.1	1.1	10.6	50	33	6.4	7.81	3.47
D3-3 LEFT	25° 29′ 13″.1 N/30° 34′ 07″.2E	15.7	26.5	9.8	15.7	9.8	5.9	3.9	2	1	9.8	52	31.4	6.9	7.54	2.51
P3-1	25° 29′ 05″.1 N/30° 34′ 05″.6E	24.7	12.3	12.3	13.6	12.3	6.2	6.2	2.5	1.2	8.6	49.4	32.1	9.9	4.99	1.98
UMD17 MS	25° 28′ 36″.9 N/30° 24′ 36″.4E	24.2	8.1	8.9	16.9	16.1	7.3	6.5	2.4	1.6	8.1	41.1	40.3	10.5	3.91	2.48
UMD17 WW	25° 28′ 36″.9 N/30° 24′ 36″.4E	31.9	10.6	12.8	8.5	6.4	6.4	6.4	4.3	2.1	10.6	55.3	21.3	12.8	4.32	1.00
D3-6 LH	25° 28′ 18″.8 N/30° 34′ 10″.4E	37.9	10.6	9.1	6.1	7.6	10.6	4.5	4.5	3	6.1	57.6	24.2	12.1	4.76	1.69
D4-2 MS	25° 25′ 13″ N/30° 31′ 17″E	22.2	11.1	13.3	15.6	13.3	8.9	4.4	1.1	1.1	8.9	46.7	37.8	6.7	6.97	3.02
P1-4 (125)	25° 20′ 13″.1 N/30° 34′ 06″.4E	30.2	9.4	11.3	3.8	11.3	9.4	5.7	1.9	1.9	15.1	50.9	24.5	9.4	5.41	1.98
P1-4 WW	25° 20′ 13″.1 N/30° 34′ 06″.4E	35.1	10.5	10.5	5.3	17.5	7	7	1.8	1.8	3.5	56.1	29.8	10.5	5.34	2.50
P2-8 RH	25° 19′ 05″.9 N/30° 31′ 24″.9E	36.5	17.5	16.1	7.3	5.8	5.1	2.9	0.7	0.7	7.3	60.1	18.2	14.4	4.17	2.00
P2-8 LH	25° 19′ 05″.9 N/30° 31′ 24″.9E	38.3	15	4	9	7.5	3	5.3	1.5	0.8	7.5	65.4	19.5	7.5	8.72	1.42
P2-8 CREST	25° 19′ 05″.9 N/30° 31′ 24″.9E	37.3	24.6	18.7	3.7	3.7	3.7	2.2	0.7	0.7	4.5	70.6	11.2	13.7	5.15	1.68
P2-8 BASE	25° 19′ 05″.9 N/30° 31′ 24″.9E	41	8.5	15.4	6	10.3	6.8	4.3	1.7	1.7	4.3	65	23.1	7.7	8.44	2.40
P2-8 MS	26° 19′ 05″.9 N/30° 31′ 24″.9E	36.8	18.4	11	5.9	11.8	5.1	3.7	1.5	0.7	5.1	66.2	12.8	15.9	4.16	3.19
P2-8 WW	25° 19′ 05″.9 N/30° 31′ 24″.9E	39.1	8.8	15.8	5.3	7	7	3.5	2.6	1.8	6.1	66.7	19.3	7.9	8.44	2.00
P2-8 INT-DUNE	25° 19′ 05″.9 N/30° 31′ 24″.9E	34.4	10.7	16.4	4.9	9.8	6.6	4.9	2.5	1.6	8.2	61.5	21.3	9	6.83	2.00
P4-2 MS (SAND SEA)	25° 16′ 42″.3 N/30° 29′ 37″.5E	26.7	13.3	9.3	13.3	9.3	5.3	5.3	2.7	1.3	13.3	49.3	28	9.3	5.30	1.75
P7 INTER DUNE	25° 14′ 55″.7 N/30° 30′ 21″.8E	24.1	9.2	11.5	13.8	11.5	11.5	6.9	1.1	1.1	9.2	44.8	36.8	9.2	4.87	1.67
P11	25° 08′ 18″.2 N/30° 33′ 05″.0E	26	13	15.6	10.4	13	7.8	3.9	1.3	1.3	7.8	54.5	31.2	6.5	8.38	3.33
P16B LH	25° 01′ 00″.3 N/30° 33′ 18″.8E	30.6	10.2	16.3	8.2	10.2	7.1	4.1	2	1	10.2	57.1	25.5	7.1	8.04	2.49
P19	24° 52′ 14″.1 N/30° 32′ 43″.8E	23.3	11.6	9.3	16.3	14	9.3	7	1.2	1.2	7	44.2	39.5	9.3	4.75	2.00
P22 BASE	24° 40′ 51″.5 N/30° 34′ 04″.8E	24.7	15.4	12.3	12.3	13.6	7.4	6.2	2.5	1.9	3.7	52.5	33.3	10.5	5.00	2.19
Average		29.31	14.27	11.48	10.29	11.00	6.79	5.11	1.86	1.31	8.20	54.62	27.44	9.73	5.93	2.21
Max		41.00	26.50	18.70	18.20	17.50	11.50	7.00	4.50	3.00	17.50	70.60	40.30	15.90	8.72	3.47
Min		11.80	7.00	4.00	3.70	3.70	3.00	2.20	0.70	0.70	3.50	41.10	11.20	6.40	3.53	1.00

S, total stable minerals; *ME*, total metamorphic minerals; *U*, total unstable minerals

Table 6 Major oxides of Kharga barchan sands

Sample	Coordinates	SiO_2	TiO_2	Al_2O_3	Fe_2O_3	MnO	MgO	Cao	Na_2O	K2O	P_2O_5	SO_3	LOI
UMD11-3	25° 44′ 19″.2 N/30° 25′ 06″.5 E	65.1	0.28	7.3	1.73	0.03	2.32	12.77	0.01	0.53	0.11	0.78	8.72
UMD13	25° 43′ 34″ N/30° 25′ 08″.9 E	62.5	0.2	6.93	1.21	0.03	2.29	18.08	<0.01	0.5	0.08	1.32	6.58
UMD15	25° 40′ 19″.28 N/30° 24′ ″.31 E	73.6	0.16	5.11	1.04	0.03	1.87	10.21	<0.01	0.32	0.01	0.8	6.58
UMD 16	25° 40′ 18″.4 N/30° 24′ 47″.5 E	50	1.19	11.5	2.8	0.07	3.35	16.45	0.39	1.12	0.13	0.94	11.79
D3-4	25° 29′ 20″.1 N/30° 34′ 25″.0 E	82.6	0.15	3.31	0.81	0.02	1.86	7.34	0.05	0.3	0.01	0.17	3.03
D 3–6	25° 29′ 36″ N/30° 34′ 0″.4 E	64.7	0.63	7.16	1.93	0.05	2.6	12.52	0.24	0.77	0.09	0.63	8.4
UMD17	25° 28′ 36″.9 N/30° 24′ 36″.4 E	55.1	0.45	10.49	2.44	0.04	2.78	17.74	<0.01	0.77	0.12	0.54	9.25
D4-2	25° 25′ 13″ N/30° 31′ 17″ E	79.4	0.19	3.57	1.08	0.03	1.74	8.92	<0.01	0.28	0.04	0.26	4.17
P1-14	25° 21′ 7″.4 N/30° 33′ 36″.8 E	82.7	0.14	2.21	0.74	0.02	1.67	7.42	0.12	0.37	0.04	0.27	3.98
P2-1	25° 19′ 29″.5 N/30° 32′ 17″.9 E	73.8	0.22	5.42	1.49	0.04	2.47	11.43	0.12	0.72	0.07	0.54	3.42
P2-3	25° 19′ 29″.8 N/30° 32′ 19″.1 E	76.8	0.16	2.23	1.2	0.03	0.81	7.3	0.35	0.4	0.06	0.38	9.95
P2-8 R	25° 19′ 05″.9 N/30° 31′ 24″.9 E	77.4	0.17	4.13	1.23	0.03	2.04	9.61	0.03	0.49	0.04	0.51	4
P2-8 L	25° 19′ 05″.9 N/30° 31′ 24″.9 E	87.4	0.1	1.98	0.7	0.02	1.38	4.03	0.08	0.29	0.01	0.3	3.42
P2-8 C	25° 19′ 05″.9 N/30° 31′ 24″.9 E	82.5	0.28	2.68	1.49	0.04	0.94	6.23	<0.01	0.4	0.04	0.46	4.62
P2-8 B	25° 19′ 05″.9 N/30° 31′ 24″.9 E	80.1	0.14	3.37	0.96	0.03	1.76	7.81	0.1	0.38	0.04	0.45	4.6
P2-8 MS	25° 19′ 05″.9 N/30° 31′ 24″.9 E	86	0.15	2.42	1.22	0.03	0.75	4.28	0.3	0.38	0.12	0.17	3.87
P2-8 WW	25° 19′ 05″.9 N/30° 31′ 24″.9 E	93	0.07	0.97	0.63	0.02	1.19	2.35	<0.01	0.09	0.01	0.22	1.12
P2-8 Inter	25° 19′ 05″.9 N/30° 31′ 24″.9 E	64.6	1.44	6.1	3.42	0.08	2.19	5	0.15	1.03	0.11	1.35	4.28
P7	25° 14′ 55″.7 N/30° 30′ 21″.8 E	74.1	0.22	5.36	1.38	0.04	1.9	10.38	0.12	0.38	0.08	0.32	5.39
P11	25° 08′ 18″.2 N/30° 33′ 05″.0 E	84.4	0.26	2.24	1.59	0.04	0.83	6.79	<0.01	0.4	0.12	0.3	2.78
P17	24° 56′ 36″.3 N/30° 35′ 10″.9 E	57.6	0.81	9.77	2.79	0.07	2.8	14.11	0.48	1.03	0.28	0.47	9.53
P21	24° 40′ 48″.8 N/30° 34′ 15″.2 E	60.7	0.66	15.14	4.21	0.05	3.41	6.13	1.3	1.66	0.19	0.67	5.56
Average		73.37	0.37	5.43	1.64	0.04	1.95	9.40	0.26	0.57	0.08	0.54	5.68
Max		93	1.44	15.14	4.21	0.08	3.41	18.08	1.3	1.66	0.28	1.35	11.79
Min		50	0.07	0.97	0.63	0.02	0.75	2.35	0.01	0.09	0.01	0.17	1.12

samples. The similarities between crest sand and slip-face sand of the linear dunes have been recorded in many dunes of other deserts (Besler 1998, 2000). These are probably due to gravity and not wind action as a dominant agent of sand transport from the crest to slip-face (Besler 1986).

Grain morphology

In the current study, the grain morphology is represented by all features of the external shape of a sand grain, including the gross form (sphericity), the roundness (sharpness of edges and corners), and the surface texture (Pye and Tsoar 2009).

Roundness and sphericity

Roundness Roundness is the least indicative texture of depositional environment because it requires a long history of abrasion to round detrital grains substantially. The roundness of sedimentary deposits is controlled by several factors, such as grain size (finer grains attain a higher degree of roundness than coarser grains of the same composition), composition (softer, more ductile, or more isotropic are more rounded than brittle, or more anisotropic grains), recycling history, and strength of the transporting agent. In conjunction with sphericity, roundness can be useful in environmental discrimination (e.g., Krumbein 1941). Currently, the aeolian sand grains become rounded by aeolian impact (Bagnold 1941). However, several publications show that some dunes contain c. 60% subangular to subrounded grains (Norris and Norris 1961). Folk (1978) mentioned that 70–90% of the dune sands were subangular to angular in the Simpson Desert (central Australia). In the Namib Desert, the majority of aeolian sand grains are subangular (Besler 1980).

The roundness of the sands of the Kharga barchans shows a unimodal distribution with a modal roundness class that varies from sub-rounded to rounded regarding the grain size, where coarser grains are much rounded than finer ones (Fig. 6A). Figure 7A shows that most of the sediments are plotted close to high R/VR in the ternary diagram of VA/A-SA/AS-R/VR of Kasper-Zubillaga (2009). The roundness of the studied sands slightly decreases from the North to south direction. The average mean roundness (ρ) of all studied quartz samples is 4.62 (subrounded-rounded; Table2). The

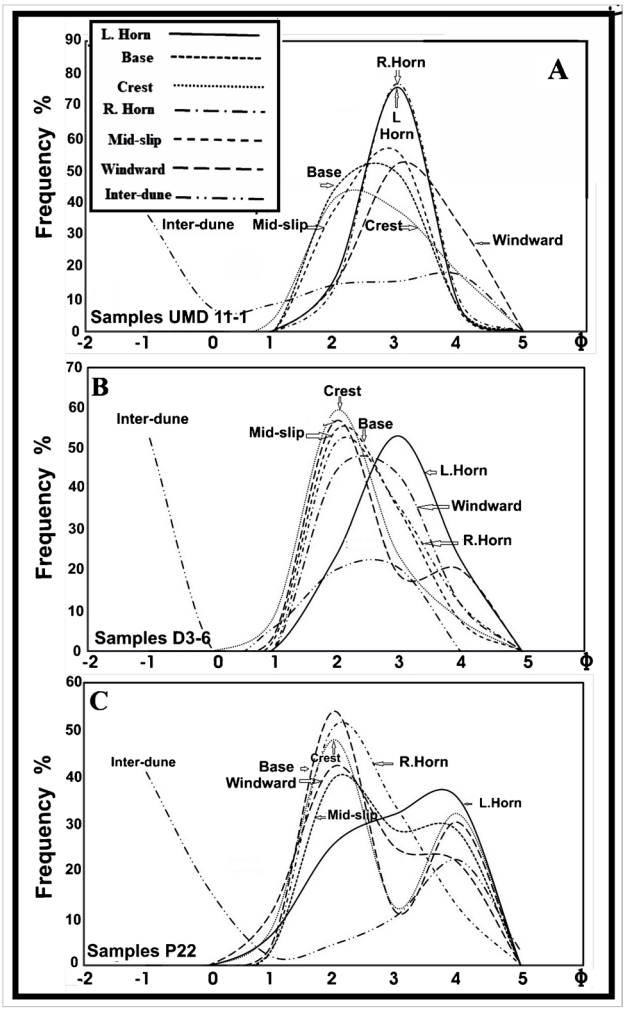

Fig. 3 Grain size distribution of the 7 sand samples from three barchans. **A** Sample UND11-1 (northern part). **B** Sample D3-6 (central part). **C** Sample P22 (southern part of Kharga dune belt)

medium-grained sands of the Kharga Depression are mostly rounded, with an average mean roundness (ρ) of 5.1. These results indicate that the Kharga sand is relatively rounded than the aeolian sand of other parts of the Western Desert of Egypt. For example, the medium-grained sand of the Great Sand Sea ranges from 4 to 4.16 (subrounded to rounded) with an average of 4.12 (Hamdan 2003). The average mean roundness (ρ) of fine grain size of the barchan dunes is 3.2 (subangular).

There is little variation in the frequency distribution of the roundness classes of the different barchans within the Kharga dune field (Fig. 6A), where the medium-grained sand has the modal class of rounded while fine-grained sands are represented by a subangular modal class. Generally, the hypothesis that the rounding in aeolian sands increases with grain size was mentioned in previous publications (e.g., Goudie and Watson 1981; Khalaf and Gharib 1985). However, revers trends were also achieved from the analysis of aeolian sands from different regions of the world, where the degree of highest rounding does not necessarily occur in coarser grains (e.g., 1–2 mm), but instead mean rounding values are relatively higher in finer sand grains (Thomas 1984; Khalaf and Gharib 1985).

There is a little variation in the roundness among different parts of the barchan, where the sands of the crest and horns seem more rounded than other parts of the barchan dunes (Fig. 6B). This is because sand grains on the windward side are moved by creep or sliding; rolling and grain impacts or collisions may be reduced. In the crest lee side and horns, fine-medium sand particles are more likely to be moved by saltation, involving grain impacts and collisions. Moreover, strong winds preferentially sort out more spherical, rounded sand grains (Mazzullo et al. 1986) more likely near the crest and brink point.

Sphericity Most workers believe that little fundamental modification to sphericity occurs after derivation from the source; inherited properties such as internal isotropism are thought to dictate the shape. Nonetheless, some dune sand shows high roundness parameters than others either because of selective sorting or because of actual modification to grain shape by environmental processes.

The studied Kharga barchan sands show that c. 85. 6% are spherical grains to very spherical grains with unimodal classes (Table 3 and Fig. 6C). Figure 6C shows very little variation in the distribution of the sphericity of the grain of different parts of an individual barchan dune (dune D2-8). Almost all samples are unimodal distribution with similar modal classes (spherical) but show a variable percentage of the modal classes (Fig. 6C); the percent of the model classes is markedly decreased on the crest sample in comparison with other parts of the barchan dunes.

Relationship between roundness and sphericity Figure 6D shows a binary relationship between the roundness and sphericity of the studied aeolian barchan sand. A strong positive correlation ($R^2 = 0.6395$) probably indicates that both roundness and sphericity are affected by the same environmental conditions. The aeolian shape sorting occurs because round and more spherical grains are more readily transported by the wind (Richardson 1903). Although, there is a distinction between roundness and sphericity (or form) as these two attributes of particle shape are independent of each other (e.g., Barrett 1980). The roundness of sand grains indicates its abrasion history while sphericity reflects the environment of deposition (Pettijohn 1957). Grain shape (sphericity and roundness) studies reflect the degree and intensity of the process of selective sorting and

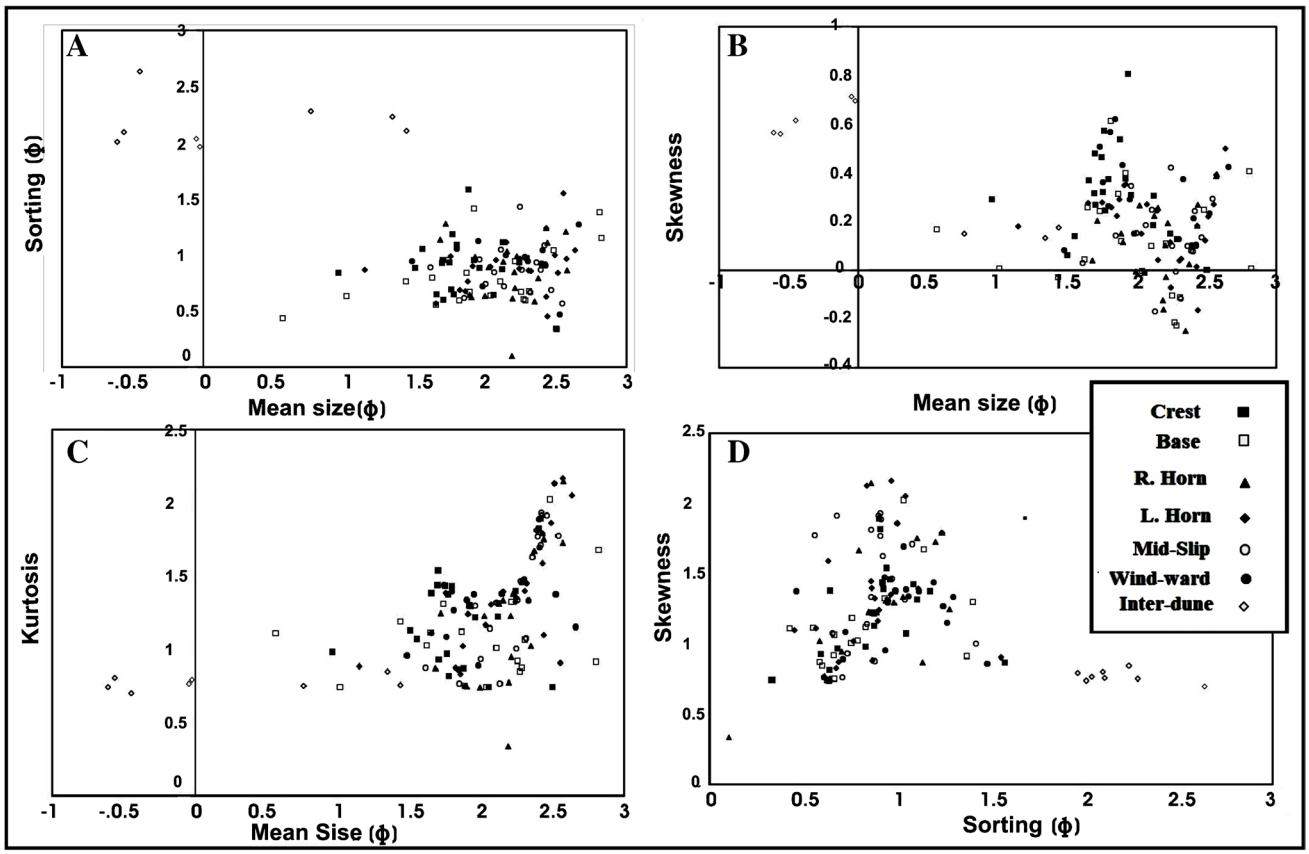

Fig. 4 Scatter diagram of the grain size parameters of Kharga barchan sands. **A** Mean size versus sorting. **B** Mean size versus skewness. **C** Mean size versus kurtosis. **D** Sorting versus skewness

may be used to differentiate depositional environments (Griffiths 1967). Generally, the dune sands have high sphericity because of selective sorting and selective transport by the wind (MacCarthy 1935; Kukal 1971; Shepard and Young 1961). On the other hand, Krumbein (1941) suggests that roundness itself is not a factor in selective sorting but indeed depends on the sphericity of transported aeolian sand grains. Kuenen (1960) observed that the degree of rounding is directly proportional to the size of the grain, degree of primary angularity, and speed of the wind. Experimental investigation shows that the well-rounded nature of the desert sands is attributed to colliding, bouncing, and wearing away of the rough irregularities during the transportation by the wind, and the spherical sand grains are transported farther by the wind than less spherical ones (MacCarthy 1935; MacCarthy and Huddle 1938; Mattox 1955; Pandey et al. 1971).

Surface features

The surface features of the sand grains of 12 samples were studied using SEM. The examined grains of Kharga sands are generally rounded to sub-rounded and some samples show sub-angular grains. The common surface features in the studied samples include mechanical (percussion pits, cracks, and conchoidal fractures) and chemical alteration and pedogenesis (diagenesis, chemical dissolution, weathering, and mineral growth) features. Some of these features are inherited from the old sedimentation history of the sand grains.

Mechanical features include pit (frost surface), disc pit, serpentine ridge, and impact scars. Frost surfaces were formed by the collision of the aeolian sand grains with each other during transportation by wind (saltation) causing the larger grains to be eroded by smaller ones (Refaat and Hamdan 2015). The resultant effect is the formation of many small irregular pits forming a frosted surface (Fig. 8A). Continuous pitting of the grain surface leads to the formation of larger disc-shaped pits which are generally concave pits with a diameter of c. 50 µm and a depth of c.10 µm–30 µm (Fig. 8B and C). Snake-like ridges are formed when two or more disc-shaped pits converge (Fig. 8E). The disc shape pits were described by Krinsley and Doornkamp (1973) and related to the action of transportation by saltation or transport by turbulent water. Percussion marks (Folk 1969) are another observed mechanical feature, which shows crescentic pits in

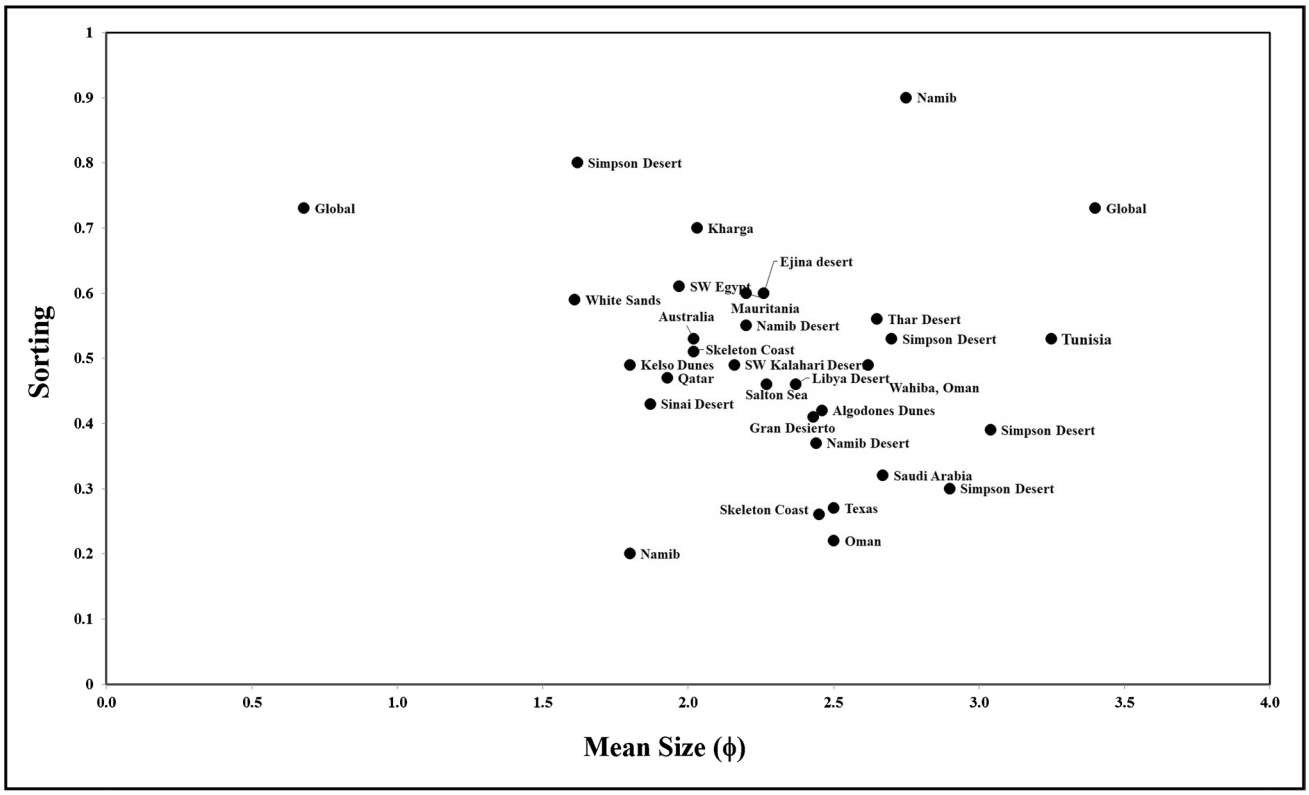

Fig. 5 Relationship between mean size and sorting of Kharga barchans and barchan sands from other deserts around the World. Taklamakan Desert (Zhu 2007); Southwestern Kalahari Desert, Namib Desert (Lancaster 1986), Gran Desierto (Lancaster 1981), Algodones Dunes, White Sands, Skeleton Coast, Salton Sea, Tunisia, Kelso Dunes, Saudi Arabia, Mauritania; Namib Desert (Lancaster 1981); Libya Desert, Canning Basin, Australia (Data in Ahlbrandt 1979); Simpson Desert (Folk 1971); Simpson Desert (Wasson 1983); Thar Desert (Goudie et al. 1973); Sinai Desert (Tsoar 1978; Zhu et al. 2014)

polished grains (Fig. 8D) and they probably result from the collision of the grains during transportation. The presence of percussion marks on particles of sand size may be used to indicate an aeolian environment (Campbell 1963). Concave or dish-shaped surfaces are smooth and younger, in some samples even cutting across older conchoidal surfaces (Fig. 8E and F). According to Krinsley and Doornkamp (1973), it is caused by aeolian fracturing in heavy sandstorms. Similar dish-shaped forms are interpreted by Le Ribault (1977) as caused by impacts in a torrential environment. Stronger chemical alteration of all older conchoidal fracture surfaces is indicated by dissolution and precipitation of silica along cleavage lines.

Surface features referring to chemical activity include corrosion marks, solution grooves and cracks, and coating on the surface of quartz grains that refers to chemical alteration and pedogenesis (Fig. 8G–L). Corrosion marks are represented by protruding contact surfaces and solution depressions and upturned plates (Fig. 8G and H). With increased chemical weathering quartz grains comprise deep angular to rounded pits with diameters of up to 40–60 µm (Fig. 8J). Other etching pattern consists of stripes or grooves of selective etching along fractures (quartz grains) or cleavage lines in feldspar grains (Fig. 8K and L). The chemical weathering of quartz grains in an arid desert environment was initiated by the large variation in temperatures between day and night. The rapid drop in temperature at night causes slowly raising the pH value to 8 or 9 of the dew water. The solubility of quartz increases with an increase in pH value.

Four coating types have been recorded in the current study; 1—sheet precipitation composed entirely of Si, with occasional upturned plates (Fig. 9A). This coating develops in response to a permanent moisture deficiency in arid desert conditions (Woronko et al. 2017); 2—smoothing grains with a thin and minor relief skin composed mainly of Si and less Fe (Fig. 9B). Smoothing grains were formed by the desert-dew cycles that start with micro-scale dissolution by dew charged with CO_2 in the night. This process is accelerated by a soluble layer of disrupted lattice quartz created by aeolian abrasion (Mahaney 2002; Besler 2008). Evaporation during the day subsequently leads to the redeposition of silica and smoothing. The same processes are described by Le Ribault (1977), who calls the result amorphization; 3—platy coating

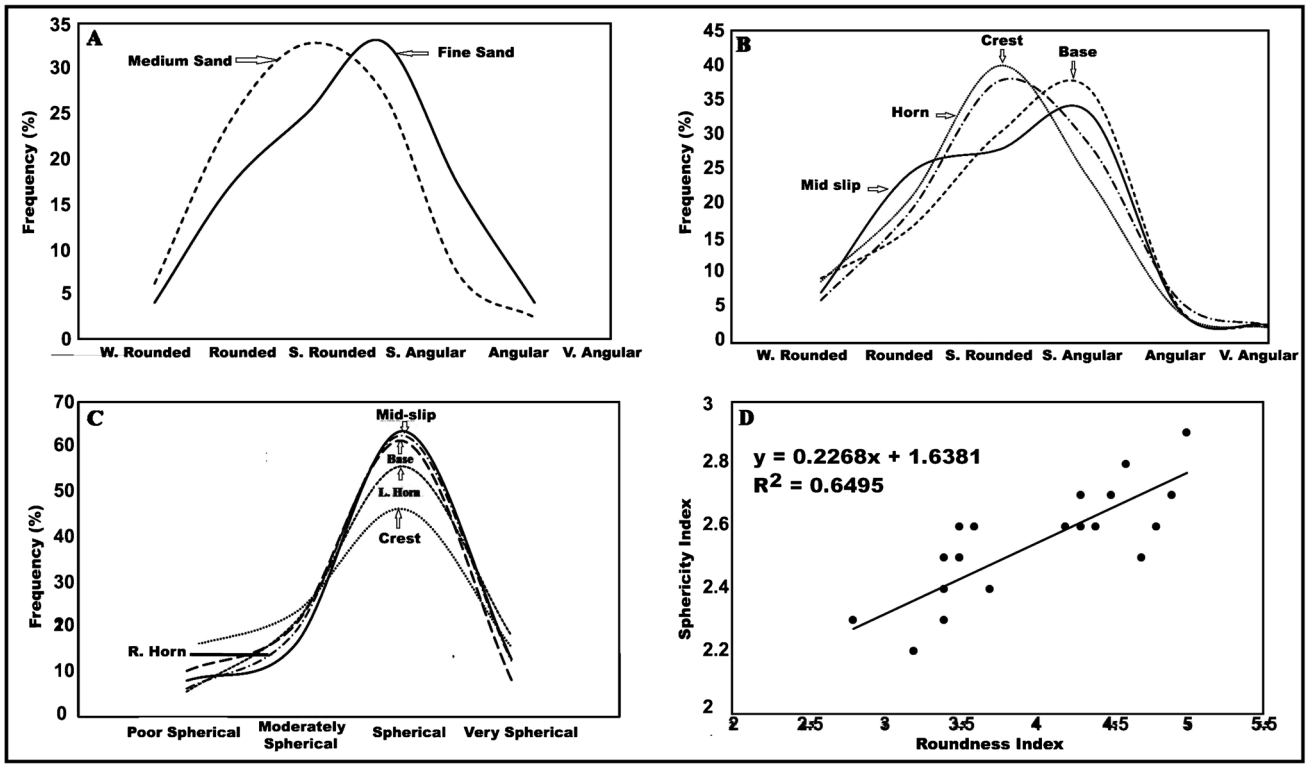

Fig. 6 **A** Frequency distribution curve of the average roundness of fine and medium grain sizes of the Kharga barchan sands. **B** Frequency distribution curves of the average roundness of the sand samples of different parts (crust, mid-slip, base, and horn) of the Kharga barchans. **C** Frequency distribution curves of the average sphericity of the sand samples of different parts (crest, mid-slip, base, and horn) of the Kharga barchans. **D** Bi-variant relationship between the roundness and sphericity indices of the Kharga barchan sands

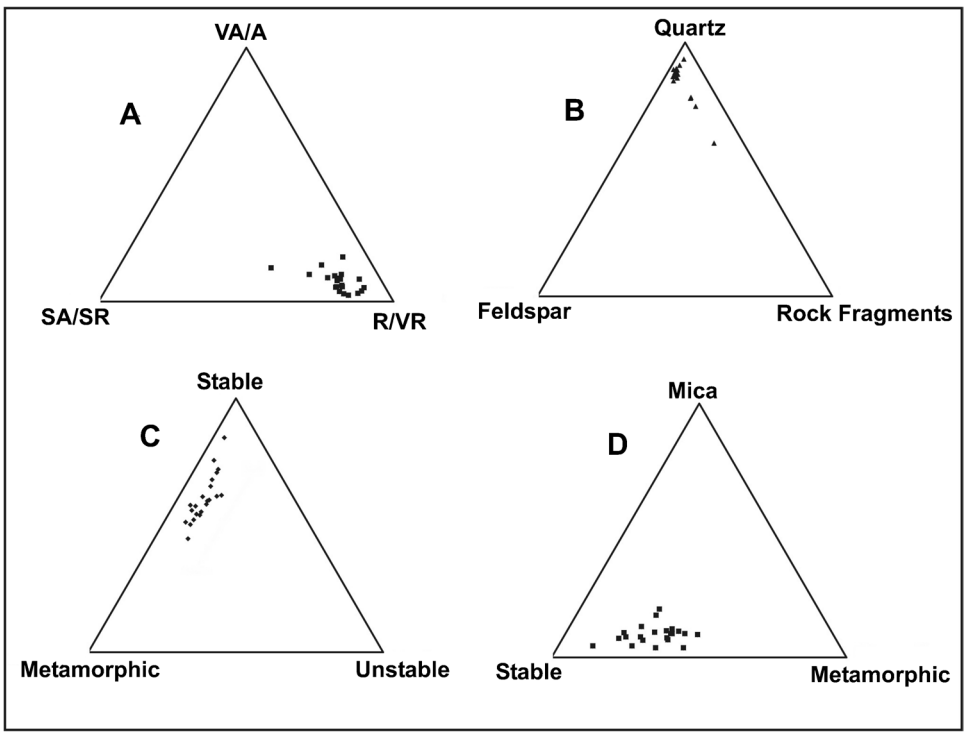

Fig. 7 **A** Ternary diagram between VA/A-SA/SR-R/VR. **B** Ternary diagram of light minerals quartz, feldspar, and rock fragments. **C** Ternary diagram of heavy minerals (stable (S), unstable (I), and metamorphic mineral grains). **D** Ternary diagram of heavy minerals (mica (MI), stable (S), and metamorphic mineral grains)

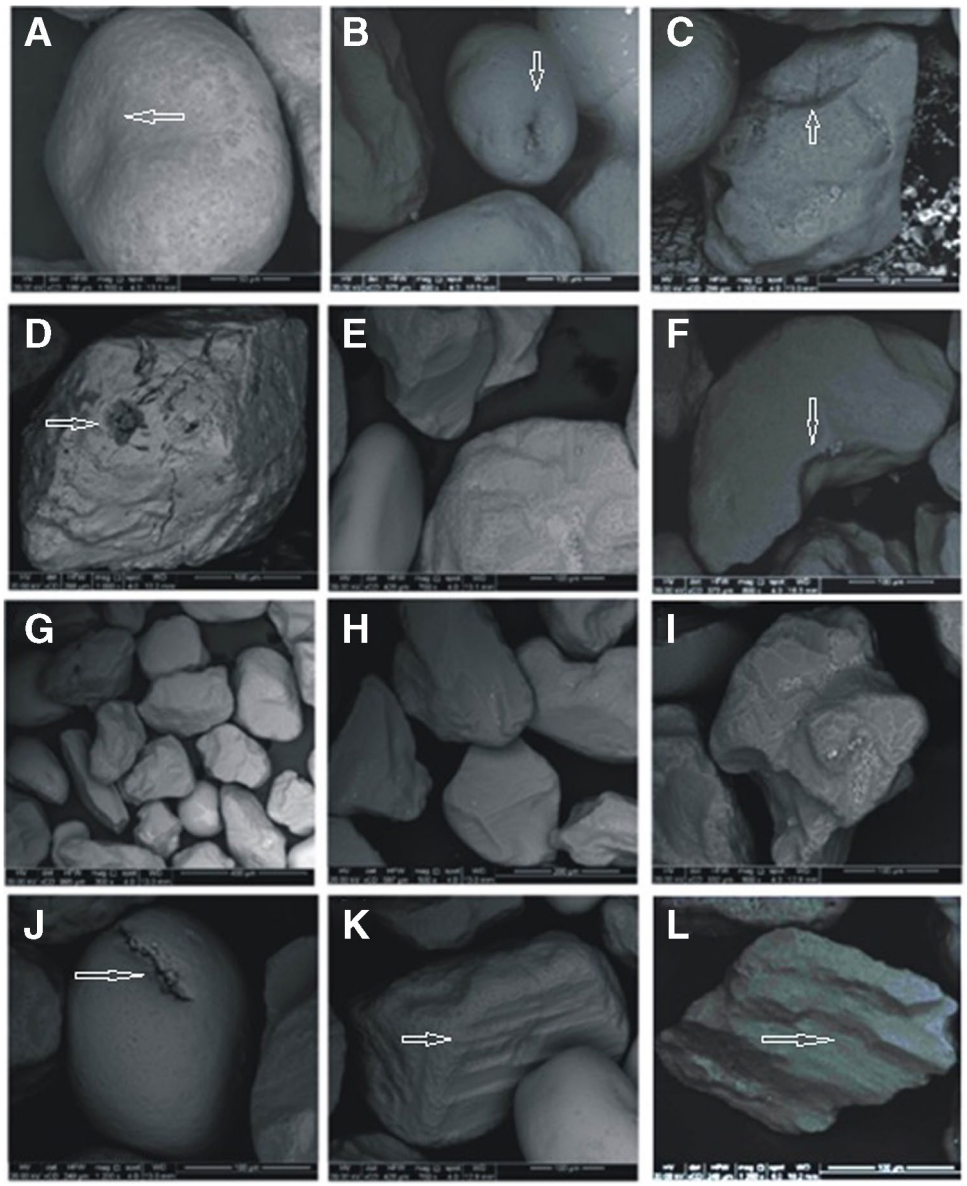

Fig. 8 Surface features of the studied barchan sands. **A** Frost surface with percussion pits. **B**, **C** disc-shaped pits. **D** Polished grain with micro-striation and percussion pits. **E**, **F** Conchoidal fractures. **G**, **H** Protruding contact surfaces and solution depressions and upturned plates. I chemically weathered quartz grain. **J** Solution groove. **K**, **L** Selective etching along cleavage lines

(Woronko et al. 2017); a morphology that in most likelihood originates under moister conditions generated in association with an abundance of clay minerals. The coating is generally composed of Si ions, but other elements such as Al, K, and Na can also be found (Fig. 9C). These grains originated in the floors of Holocene playa lakes in the northern reaches of the Sahara region (Woronko et al. 2017). 4—Some grains are partially coated by evaporite minerals such as gypsum and halite (Fig. 9D).

Mineralogical characteristics

Thirty-one samples of the sand of Kharga barchans have been subjected to a detailed mineralogical investigation for their light and heavy mineral compositions.

Light minerals

Microscopic investigations of the aeolian sands revealed that they are composed mainly of quartz together with feldspars and subordinate rock fragments (Table 4 and Fig. 7B).

Quartz is the essential component of the sands of the Kharga barchan dunes. Two types of Quartz grains have been identified: monocrystalline and polycrystalline quartz. Monocrystalline quartz (MQ) constitutes an average value of 74.60% with a range from 63.9 to 82.8% (Table 4). Monocrystalline Quartz includes three varieties: straight extinction (MS); undulose (wavey) extinction (MU); and monocrystalline quartz with inclusions (MI) (see. Blatt and Christie 1963; Kasper-Zubillaga 2009). MS predominates and displays a mean value of 54.62% and ranges from 33.8 to 65.5%. MI represents only 6.8% of the whole counted light minerals. The monocrystalline quartz with

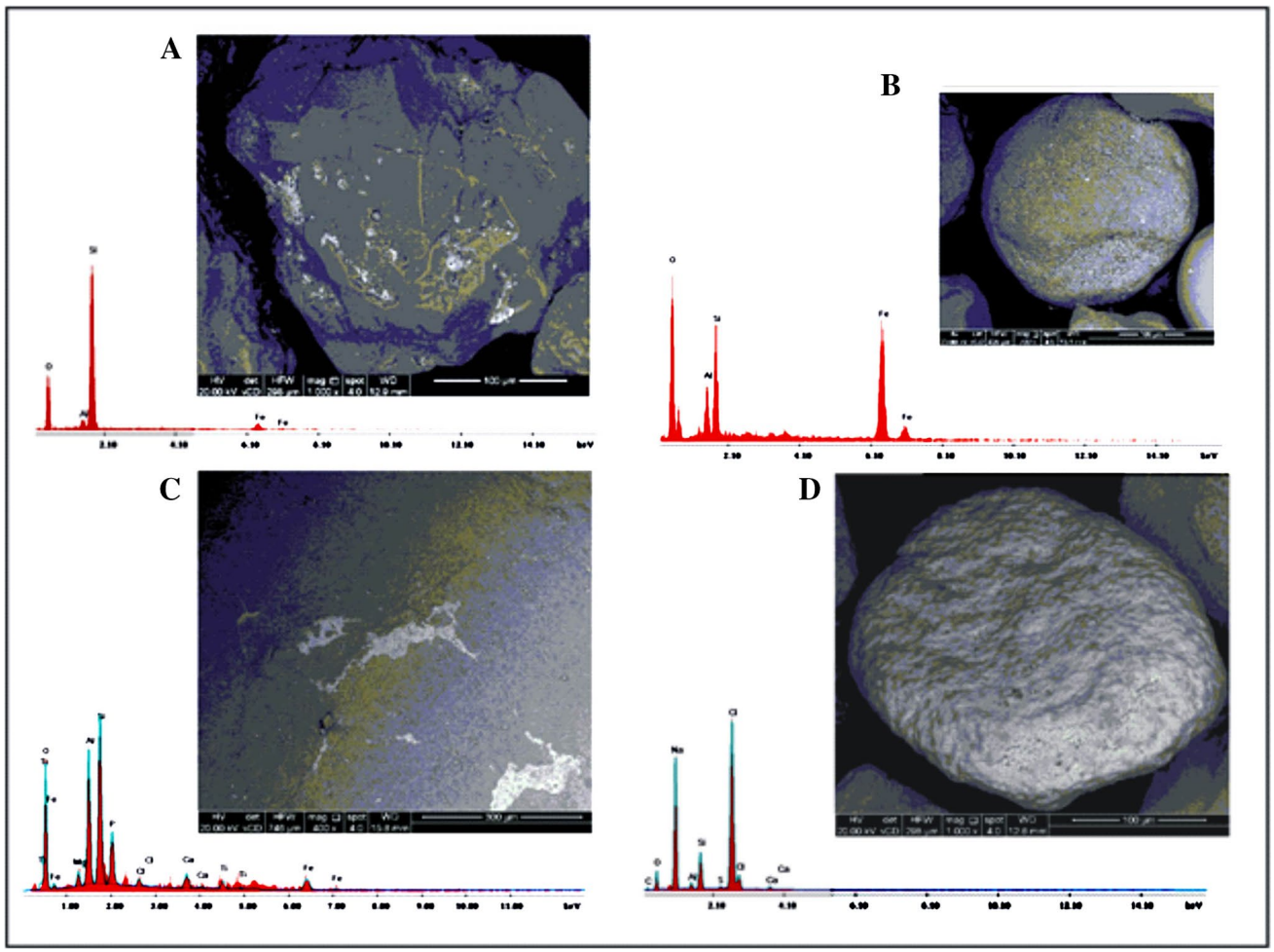

Fig. 9 Coating of quartz grains of Kharga barchan. **A** Sheet precipitation composed entirely of Si. **B** Thin and minor relief skin composed mainly of Si and less Fe. **C** Clay coating is generally composed of Si ions with other elements such as Al, K, and Na. **D** Traces of evaporite minerals such as gypsum in the coating

undulose extinction (MU) ranges from 8.4 to 15.5%, averaging 12.54%. Previous publications recorded the dominance of monocrystalline quartz in the aeolian sand of the Western Desert of Egypt (Hamdan 1987, 2003; Hamdan and Refaat 1999; Besler 2000). Composite or polycrystalline quartz grains represent the least constituent types of quartz grains with an average percentage that varies between 7.5% and 15% (Table 4). Table 4 shows also that the aeolian sand of Kharga barchan sands contains much quartz with undulose extinction (MU) and polycrystalline quartz grains than those in other parts of the Western Desert (Hamdan 2003; Besler 2000).

Feldspars range from 3.7 to 11.4% with an average value of 8.92% (Table 4). K-feldspars (orthoclase and microcline) are more common with an average value of 5.17%. Plagioclase attains an average value of 3.74% of the whole counted light minerals (Table 4). The average feldspar of Kharga barchan sands is comparable with those of northern Egypt (Hamdan and Refaat 1999) and slightly lower than those of the Great Sand Sea (Hamdan 2003; Besler 2008).

Rock fragments percentage is very few in the studied aeolian sands with an average value of 5.55% and represented mainly by limestone and shale fragments. Some samples contain high contents of rock fragments, e.g., sample UMD 13 windward that attains c. 32% of the whole counted light minerals (Table 4). The counted rock fragments are higher than that recorded by Hamdan (2003) in the southwestern Western Desert.

Heavy minerals

The heavy mineral assemblage of the sands of Kharga barchans consists of three categories: stable minerals (zircon, tourmaline, and rutile), metamorphic minerals (garnet, andalusite, and staurolite), and unstable minerals (pyroxene, epidote, and amphiboles (Fig. 7C). Opaque minerals are not counted in this study. Zircon is represented by euhedral prismatic colorless grains with less abundant yellow, varying between 11.8% (sample UMD12 L. horn) and 41% (sample

P2-8 base) with an average value of 29.4% of all non-opaque heavy minerals. Zircon content is nearly similar to that of the aeolian sands of the Great Sand Sea (Hamdan 2003). Tourmaline grains vary between 7% (Sample UMD12) and 26.5% (Sample D3-3) with an average value of 14.39% of the total non-opaque heavy mineral content (Table 5). Rutile grains range from 4% (sample P2-8 windward) and 18.7% (sample P2-8 crest), with an average value of 11.5% (Table 4). The stable minerals usually constitute the main component of the heavy mineral content in both the Nubian sandstone bedrock and the ancient aeolian sands (Hamdan 2003; Besler 2008).

Metamorphic minerals are represented mainly by staurolite and garnet with very low percentages of sillimanite. Staurolite grains vary between 3.7% (sample P2-8 crest) and 18.2% (sample UMD10-2) with an average value of 11% of the total content of non-opaque minerals (Table 5). Garnet ranges from 3.7% (sample P2-8 left horn) to 7.5% (sample P1-4 windward), averaging 6.8% (Table 4). Metamorphic mineral grains are also abundant in the Nubian sandstone bedrock, but they are less abundant in ancient alluvial deposits.

The unstable minerals are represented mainly by epidotes and pyroxenes and are less common by amphiboles. Epidote is recorded in most studied samples averaging 5.1% and ranging from 2.2% (sample P1-4 windward) to 7% (sample P2-8 crest). Pyroxenes and amphiboles are mainly represented by augite and hornblende with average values of 1.3% and 1.9%, respectively (Table 5). Mica is represented by biotite and muscovite grains attaining an average value of 8.2% and varies between 3.5 (P1-4 windward) to 17.5% (sample UMD12 left horn). Most of the counted mineral grains are plotted close to the corner of the stable mineral grains of a ternary relationship between mica, stable, and metamorphic mineral grains; however, some samples contain a considerable amount of either mica or metamorphic minerals (Fig. 7D). There is a strong negative correlation ($R^2 = 0.6512$) between stable and unstable mineral grains (Fig. 10A) and a very weak positive correlation ($R^2 = 0.0899$) between metamorphic and unstable mineral grains (Fig. 10B).

The ratios of stable to unstable heavy minerals of Kharga sands range from 3.53 to 8.72 with a mean value of 5.93% for all studied samples compared to less than 2 at most other localities in the Western Desert of Egypt (Table 5). The ratios of garnet to epidote vary between 1 to 3.47 with an average value of 2.6 (Table 5) which is less than the same ratios in most other localities in the Western Desert of Egypt.

Geochemical analysis

The major oxides composition of 22 samples of Kharga barchan sands is shown in Table 6 and the correlation matrix of the major elements is cited in Table 7. SiO_2 is the main oxide forming the dune sand samples, which ranges from 50% (sample UND 15) to 93.0% (sample P2-8 windward), averaging 73.4% of the whole composition. This value seems to be close to the average world value of sandstones (Turekian and Wedepohl 1961) and relatively is lower than the average SiO_2 values of the dune sand of the southwestern Western Desert (85.6%; Hamdan 2003). Table 7 shows clearly that there are clear negative correlations between SiO_2 and most major oxides, which probably indicates different sources of the studied aeolian sands. SiO_2 is negatively correlated with other major elements (Table 7; Fig. 11A), probably due to the abundance of SiO_2 being controlled by the increase in the compositional maturity, where in fact the increase in compositional maturity the percentage of SiO_2 increases and the percentage of other major elements decreases.

Fe_2O_3 vary between 0.63% (sample P2-8 windward) to 4.21% (sample P21) with an average value of 1.6% (Table 6). Fe_2O_3 shows a strong positive correlation with TiO, and MnO. Na_2O and CaO (Table 7) and is slightly higher than the world value of sandstones (1.38%; Turekian and Wedepohl 1961). Generally, iron oxide exists in different forms: (1) a thin hematite coating on the quartz grains as multiple layers of clay stained by iron oxides (see Besler 1998); (2) it also fills the cavities on the eroded quartz and feldspar grains; (3) as detrital opaque grains (e.g., magnetite and ilmenite). The existence of ilmenite is indicated by the presence of considerable amounts of TiO_2 in some samples and their positive correlations with Fe_2O_3 (see Table 7 and Fig. 11B).

Al_2O_3 is positively correlated with most other major oxides except SiO_2 (Table 7). It ranges from 0.97 to 15.14% with a mean value of 5.43% (Table 6). The average value seems a little higher than those of the aeolian sands of the Great Sand Sea (4.7%; Hamdan 2003). The positive correlation between the Al_2O_3, K_2O, Fe_2O_3, and TiO_2 in the studied samples probably indicates that Al_2O_3 content is related to the existence of K-feldspars and detrital biotite grains, respectively (Fig. 11C and D).

Homogeneity of Kharga dune field

Textural homogeneity

The homogeneity of the sands of the Kharga dune field has been tested using the variation of the textural parameters (grain size, grain shape, and surface features) of the barchan sands in the north–south direction. Theoretical and empirical studies have shown that grain-size distributions of aeolian sand deposits change along their transport paths (McLaren 1981; Lancaster 1995; Pye and Tsoar 2009). For example, parabolic dune fields show a gradual and slight decrease in particle-size means with downwind distance due to the winnowing

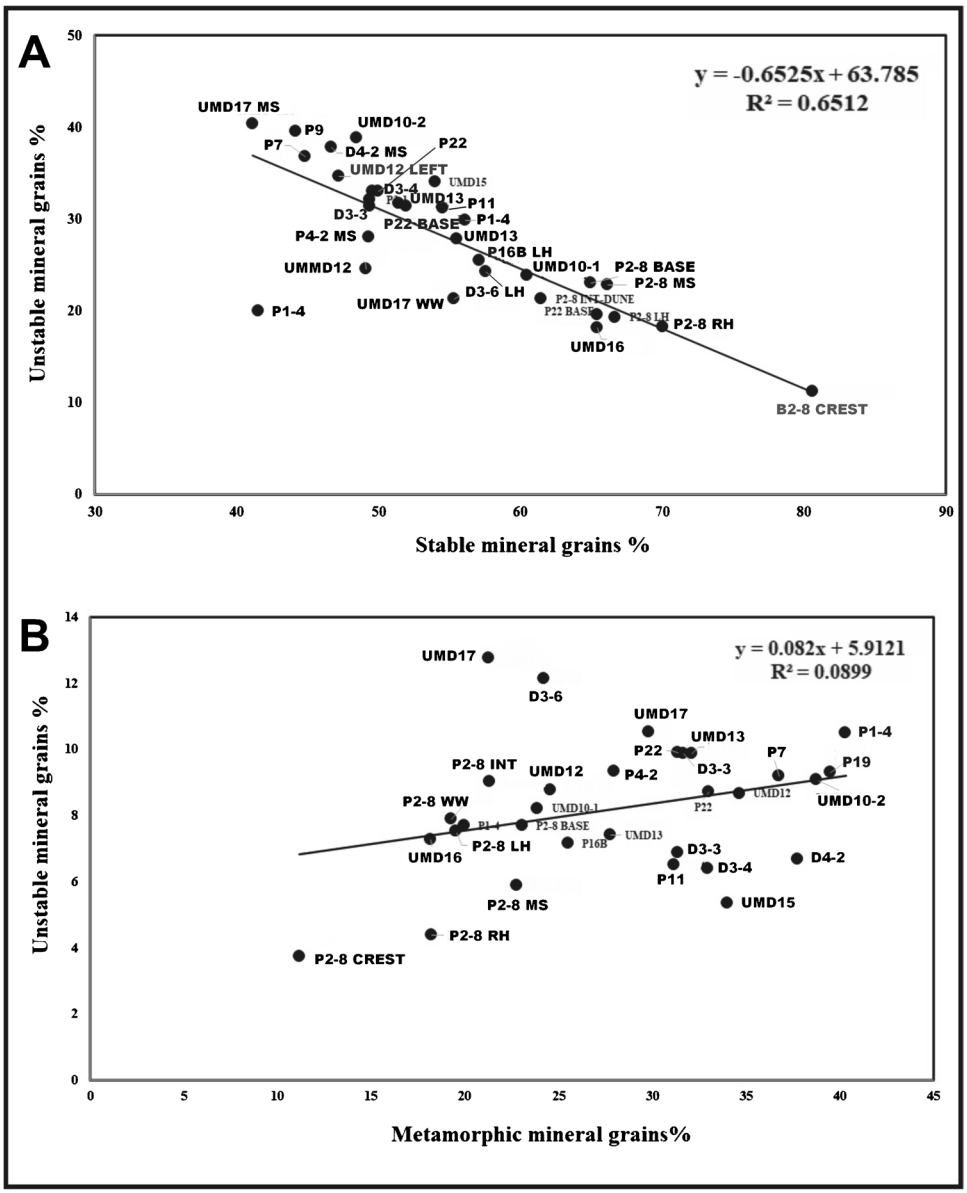

Fig. 10 **A** scattered diagram of the stable mineral grains versus unstable minerals of the Kharga barchan sands. **B** Unstable mineral grains versus metamorphic minerals of the Kharga barchan sands

Table 7 Correlation matrix of Kharga barchan sands

	SiO_2	TiO_2	Al_2O_3	Fe_2O_3	MnO	MgO	CaO	Na_2O	K2O	P_2O5	SO_3
SiO_2	1										
TiO_2	−0.71	1.00									
Al_2O_3	−0.90	0.62	1.00								
Fe_2O_3	−0.76	**0.83**	**0.85**	1.00							
MnO	−0.71	**0.94**	0.62	**0.84**	1.00						
MgO	−0.86	**0.60**	0.91	0.69	0.56	1.00					
Cao	−0.86	0.56	0.60	0.44	0.56	0.67	1.00				
Na_2O	−0.40	0.39	0.66	**0.71**	0.41	0.47	−0.08	1.00			
K_2O	−0.78	**0.77**	**0.90**	**0.96**	**0.77**	0.79	0.44	**0.79**	1.00		
P_2O_5	−0.66	0.59	**0.71**	**0.78**	**0.71**	0.52	0.41	**0.61**	**0.75**	1.00	
SO_3	−0.68	0.62	0.51	0.51	0.55	0.52	0.73	0.08	0.50	0.24	1.00

Numbers in bold refer to highest correlation elment oxides

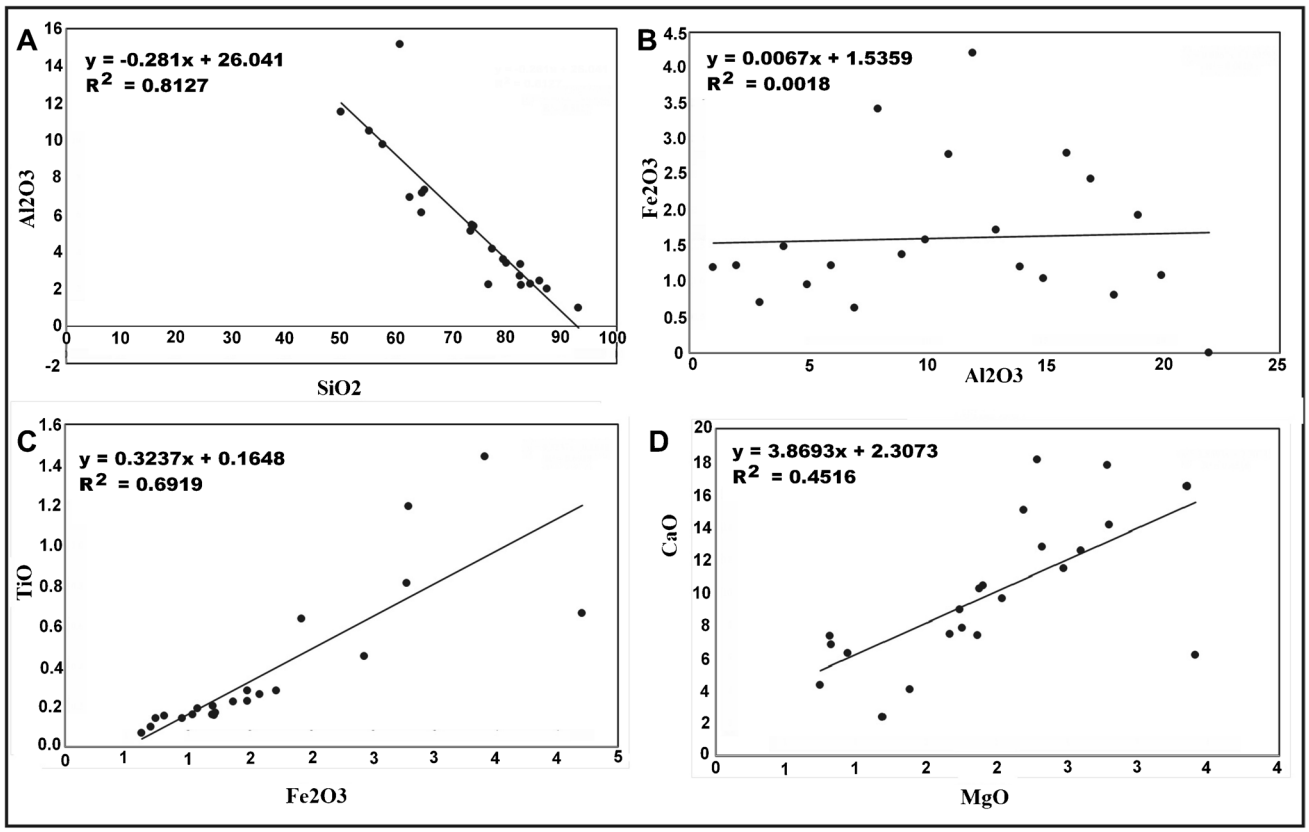

Fig. 11 Scattered diagram of the major oxides of the Kharga barchan sands. **A** SiO_2 versus Al_2O_3. **B** Al_2O_3 versus Fe_2O_3. **C** Fe_2O_3 versus TiO. **D** MgO versus CaO

of coarse sands (Roskin et al. 2014), no significant trends have been indicated for active linear dunes (Lancaster 1995), and almost no published data for barchan dunes. In the present study, there is a gradual and slight increase in the mean size from the north to south direction (Fig. 12A), and there no significant trends have been identified in the sorting of the Kharga sands (Fig. 12B). We conclude that the north–south coarsening trend of the Kharga barchan belt is related to the contribution of coarse sand grains from the Nubian sandstone which is well exposed in the middle and southern part of the

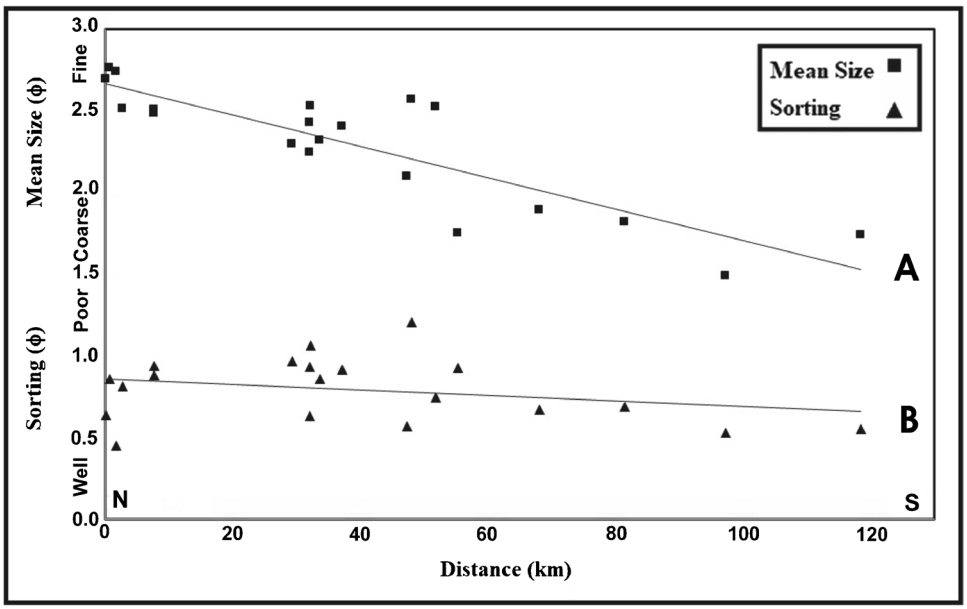

Fig. 12 Textural variation (from north to south) along Kharga barchan field. **A** Variation of mean size (Mz). **B** Variation of sorting

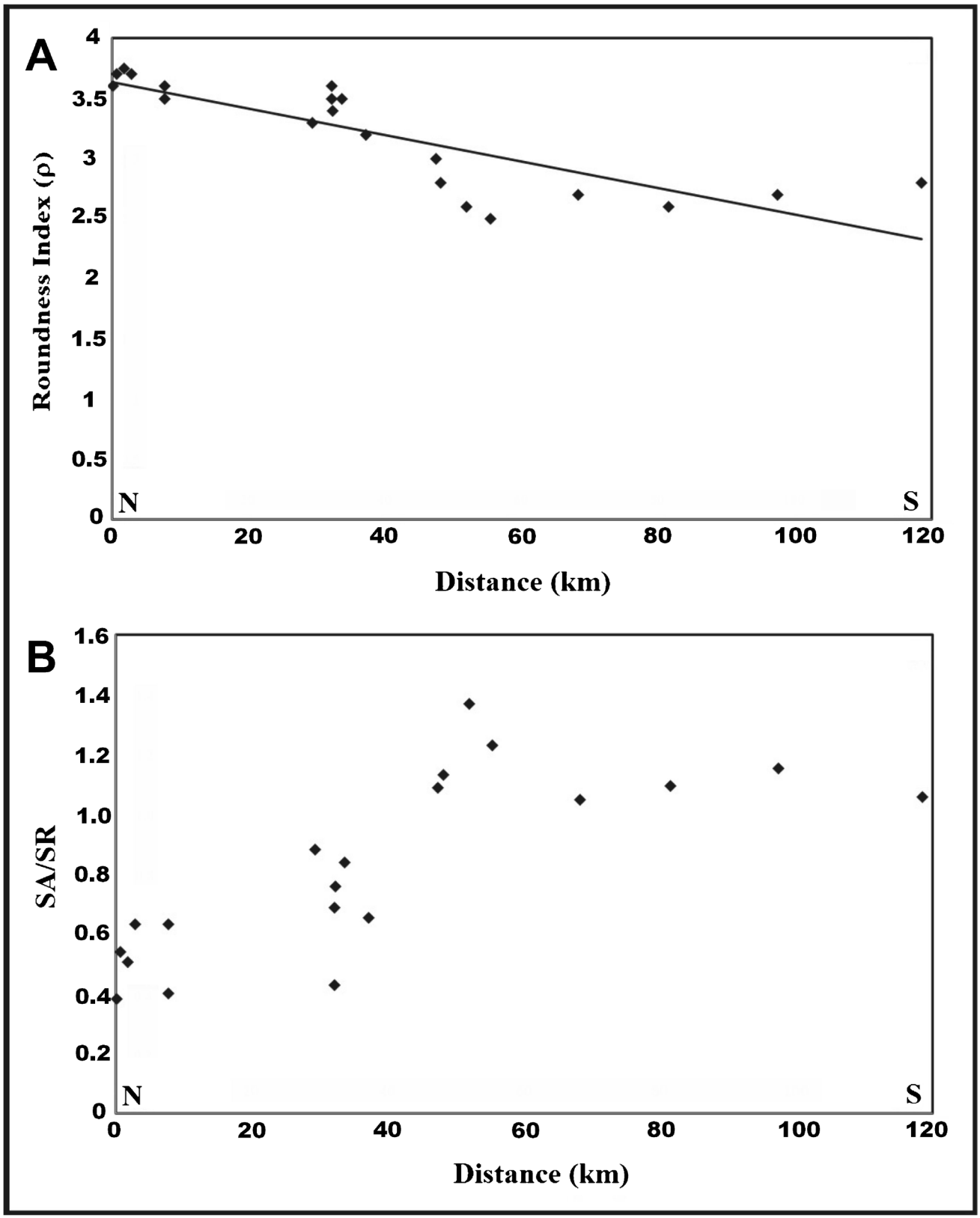

Fig. 13 Variation of roundness (from north to south) along Kharga barchan field. **A** Variation of roundness index (ρ). **B** Variation of SA/SR ratios. Samples as in Table 3

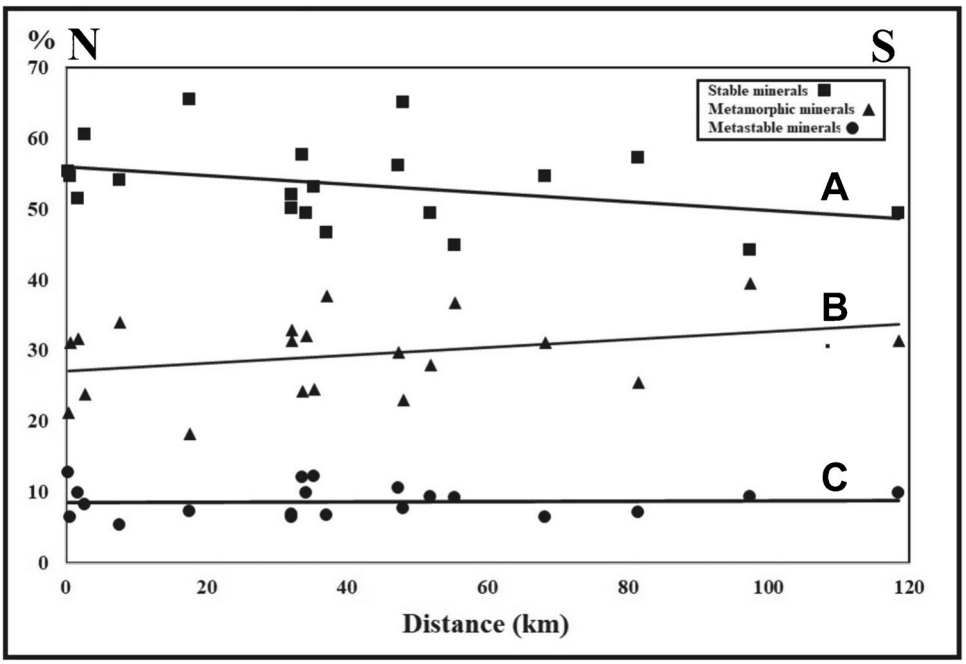

Fig. 14 Variation of mineralogy (from north to south) of the Kharga barchan sands. **A** Variation of stable minerals. **B** variation in metamorphic mineral grains. **C** Variation in unstable minerals. Samples as in Table 6

Table 8 Grain size characteristics of the proposed sources of Kharga barchan sands

Proposed source	Age	MZ	Sorting	Skewness	Kurtosis	
Nubian sandstone	U. Cretaceous	0.99	1.21	−0.06	0.52	Hamdan et al. 2015
Moghra sandstone	L. Miocene	2.22	0.66	0.12	0.56	Hamdan et al. 2015
Alluvial sand	Pleistocene	2.25	1.64	0.71	1.80	Hamdan 1987
Ancient dune	Pleistocene	1.83	0.72	0.05	0.96	Current work
Playa	Holocene	3.13	1.98	0.51	2.67	Current work
Nile sands	Pleistocene Holocene	2.7	2	1.7	1.7	Hamdan et al. 2019

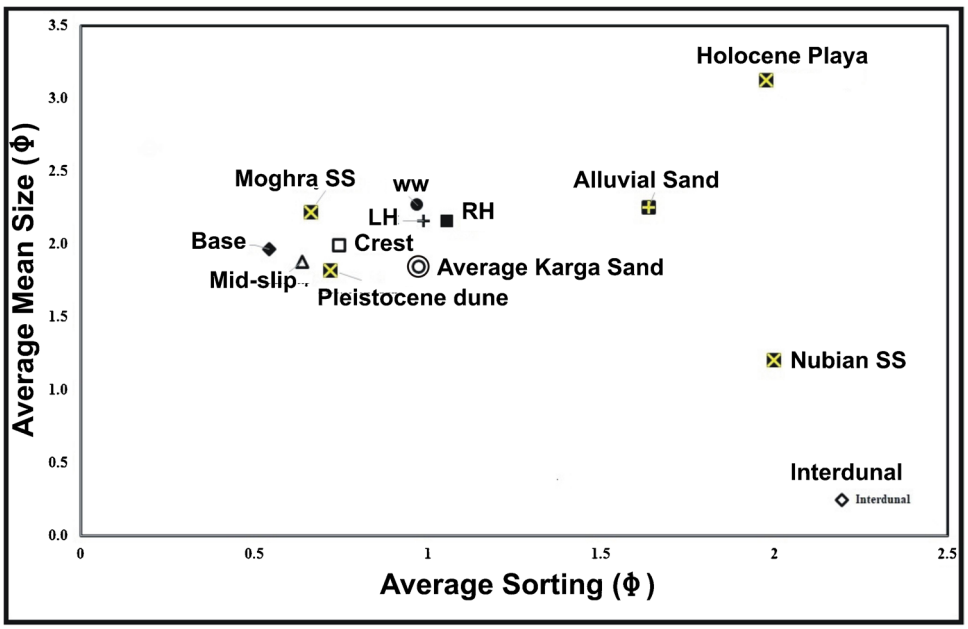

Fig. 15 Scattered diagram of average sorting versus the average mean size of the Kharga barchan sand and proposed sources in the Western Desert of Egypt

Kharga Depression (Fig. 1). We also believe that the grain size fractionation (Roskin et al. 2014) has little influence on the grain size homogeneity of the Kharga barchan belt, where the fine sand fraction increases southward parallel to the wind direction. This is reflected in the high skewness values in the samples of the middle and southern parts of the Kharga Depression (see Table 1). Figure 13A shows the variation in the roundness index (ρ) of the studied aeolian sand grains with a distance from north to south direction. The values of the roundness index (ρ) are relatively homogeneous and slightly decrease (more angular) in the samples of the middle and southern parts of the Kharga barchan belt, while the sand in the northern part of the Kharga Depression show a variable roundness index and is relatively high (ρ). The change from better to less rounded sands is recorded at c. 50 km from the northern escarpment corresponding to the exposure of Nubian sandstone (Figs. 1 and 13A). The SA/AR ratios of the studied sands are also high in the middle and southern parts of the Kharga depression in comparison to the samples of the Northern part (Fig. 13B).

Mineralogical homogeneity

A considerable variation in the stable and metamorphic mineral grains has been noticed in a trend parallel to the prevailing wind (Fig. 14A and B). The percent of the stable mineral grains shows a slight decrease southward while there is a significant increase in the metamorphic mineral grains in the samples of the middle and southern parts of the depression (Fig. 14A). We believe that the slight decrease in the stable minerals is probably related to the remarkable increase of metamorphic minerals grains and mica (Table 5). Nonetheless, the increase of metamorphic grains in dune sands of the middle and southern parts of the depression is related to the contribution from Nubian sand sources which are characterized by a high percent of metamorphic mineral grains (Shukri and Ayouty 1953). Unstable minerals grains show no significant trend from the north to south direction (Fig. 14C).

Geochemical homogeneity

The major elements of the Kharga barchan sand show no significant trend from the north to the south direction of the dune field. However, the CaO, Al_2O_3, and alkali oxides (K_2O, Na_2O) display a significant distribution in the Kharga dune field. which is controlled by the exposure of the bedrock on the floor of the depression. High CaO content reflects the abundance of carbonate sand grains in the barchan sand samples near the upper Cretaceous Tarawan chalk exposures (see Fig. 1, Table 6). On the other hand, the high content of Al_2O_3 and alkali oxides is related to the existence of shale flakes in the sand samples near the Upper Cretaceous Dakhla shale exposures (see Fig. 1, Table 6).

Table 9 Heavy minerals of the proposed sources of Kharga barchan sands

	Age	TO	RU	ST	GA	EP	PX	S	Met	U	S/U	GA/EP	Reference
Nubian sandstone	U. Cretaceous	6.80	6.99	29.45	39.31	4.04	1.64	28.73	68.76	5.68	5.47	9.7	Hamdan et al. 2015
Moghra sandstone	L. Miocene	15.04	6.48	21.18	14.67	27.42	0.58	32.23	35.85	28.00	0.73	0.5	Hamdan et al. 2015
Alluvial sand	Pleistocene	23.88	11.56	11.93	9.53	3.51	5.57	49.56	21.46	9.08	1.35	2.7	This Work
Ancient dune	Pleistocene	20.54	1.73	16.25	22.29	9.08	0.92	46.72	38.50	9.91	1.55	2.5	Hamdan 1987
Playa	Holocene	22.90	9.01	11.96	11.99	2.04	7.37	47.06	23.94	9.41	1.20	5.9	Hamdan 1987
Nile sands	Pleistocene to Holocene	2.01	1.73	2.62	3.21	1.57	4.0	3.74	4.98	91.28	0.04	0.8	Hamdan et al. 2019

S, stable; *Met*, metamorphic; *U*, unstable

Some sand samples show high contents of CaO and Na_2O along with SO_4 probably related to the existence of evaporite grains such as gypsum (CaSO4) and halite (NaCl). The sand of these samples is likely subjected to high evaporation and a relatively higher level of groundwater close to the newly reclaimed fields.

The provenance of the sands of Kharga barchan dunes

Texture proxy

The Kharga barchan sands are mainly medium to fine-grained (average Mz is 2.11 Φ), which is similar to the mean size of the sands of the dune belt in northern Egypt (El Gammal and Cherif 2006; Embabi et al. 2012) and at Toshka to the south (Hamdan et al. 2015). The measured mean size of the Kharga sands is coarser than other dune sands of the Western Desert. This probably indicates that both Toshka and Abu Muharak dunes belong to the same source on one hand but differ from the sources of other dune sands of the Western Desert, of Egypt. There are at least six proposed sources of the sands of the Abu Muharak barchans in the Kharga Depression; these are Upper Cretaceous Nubian sandstone, Lower Miocene fluvio-marine Moghra sandstone, Pleistocene fluvial sand, ancient (Pleistocene) dunes, Holocene alluvial and lacustrine (playa) sands, and Nile sediments. All these proposed sources are existed in the Western Desert in general and in Kharga Depression in particular, except the Moghra sandstone which is exposed in the northern part of the Western Desert while the Nile sediments exist on the high terrace along the Nile Valley and Nile Delta. There are several differences in the average grain size parameters of the sands of these proposed sources (Table 8). The early Miocene Moghra sands in northern

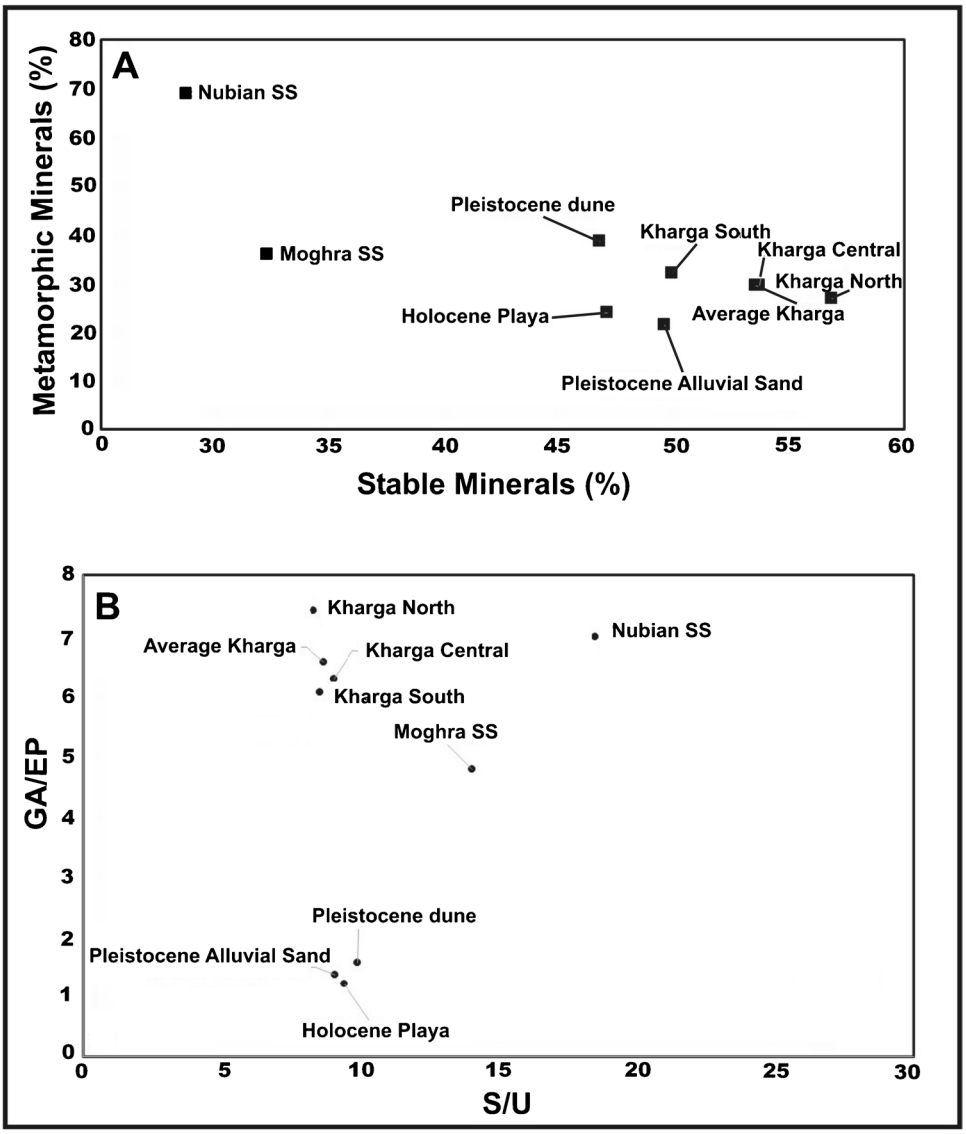

Fig. 16 **A** Scattered diagram of stable mineral grains versus metamorphic mineral grains of the Kharga barchan sands and proposed source of the Western Desert of Egypt. **B** Stable/unstable ration versus garnet/epidote of the Kharga barchan sands and the proposed sources of Western Desert of Egypt

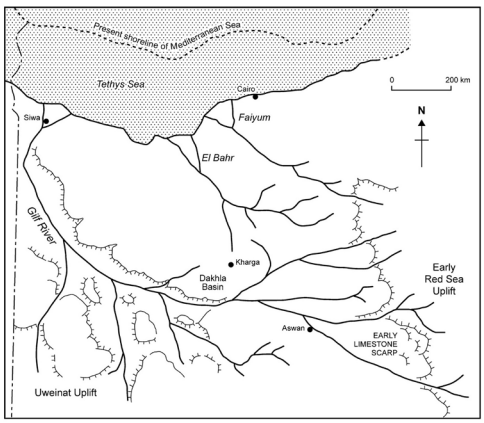

1- Mid-Tertiary uplift of Red Sea Mountains & Uweinat and humid climate

Nubian Sandstone
(Hamdan et al., 2015)
Rich in metamorphic mineral grains

Moghra Sandstone
(Hamdan et al., 2015)
Rich in unstable mineral grains

2- Late Tertiary Humid climate

Radar Rivers
McCauley et al., 1982

Siwa Oasis
Qattara Depression
Aeolian sand at Qattara-Siwa area (Hamdan and Refaat, 1999

3- Early-Middle Pleistocene (humid to semiarid climate)

Inverted Wadis
(Giegengack, R., Zaki A. 2017)

4- Late Pleistocene (Hyper-arid Climate)

Selima Sand Sheet
(Maxwell, &Haynes, 2001)

Longitudinal Dune (Draa)
Besler, 1998

5- Early Holocene (Humid climate), fluvial and lacustrine activity

Nile Sediments
(Shukri, 1950)
Rich in unstable mineral grains

Stabilized dune
(Besler 1998)
Rich in stable mineral grains

Playa Sediments
(Hamdan 1987)
Rich in metamorphic and stable mineral gains

Alluvial deposits
(Hamdan, 1987)
Rich in stable mineral grains

ıte Holocene (Hyper-arid climate), wind activity

Kharga Dune sands
(current study)
Rich in stable, little metamorphic and rare unstable mineral grains

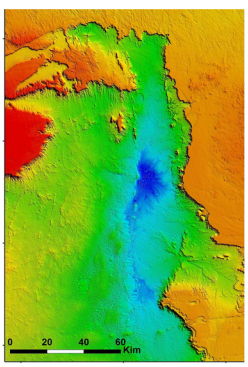

◂**Fig. 17** Schematic diagram demonstrating the possible sources of the aeolian dune sand at Kharga Depression. The Mid-Tertiary map is modified after (Hamdan and Hassan 2020); Pleistocene and Holocene stages are modified after Hamdan et al. 2015

Egypt are characterized by fine sand grain size (Mz = 2.22 Φ), well-rounded quartz grains, better sorted (σ = 0.6 Φ), and the existence of thick shale layers (Hassan et al. 2012). The Nubian sandstone, on the other hand, consists of angular to subangular, coarse-grained sand (Mz = 0.99 Φ), worse sorting (σ = 1.21 Φ) with abundant conglomeratic layers, and a lack of shale layers.

Figure 15 is a scatter diagram of the average mean size and sorting of the Kharga barchan sands and the proposed sources. The studied barchan samples are plotted with the Moghra sandstone, ancient (Pleistocene) dune sands in one field, and the average values of the Pleistocene alluvial sand and Holocene playa sands in the near field. On the other hand, the average values of the Nubian sandstone samples are plotted far from the Kharga barchan sands. Thus, the Moghra sandstone was most likely the main source of Abu Muharak dune belts. Nevertheless, the relatively coarser mean size of the Kharga sands, as well as low mean roundness, probably indicates that the Nubian sandstone, alluvial sand, and the playa sand, probably contribute, as a secondary source, to the sand of the Abu Muharak dune field in the Kharga Depression.

Mineralogical proxy

Table 9 shows the heavy mineral assemblages of the samples of the proposed sources; the Nubian sandstone is characterized by a high content of metamorphic mineral grains while those of Moghra have a high amount of stable and unstable mineral grains. The Nile sediments are very rich in unstable minerals grains (Shukri 1950a, b). Pleistocene sands (alluvial, aeolian) and Holocene playa are rich in stable heavy mineral grains (Table 9). The mineralogical composition of the studied aeolian sands is represented by quartz, opaque minerals, stable heavy minerals, metamorphic minerals, and unstable minerals. They also contain a considerable amount of wavy and polycrystalline quartz grains which are existed in the Nubian Sandstone (Shukri and Ayouty 1953). The bi-variant relationship between the stable minerals and the metamorphic minerals of the studied aeolian sand along with the proposed sources is given in Fig. 16A. The Kharga barchan sand is plotted in one field along with the samples of the Pleistocene dune sand and alluvial sand and not so far from the Moghra samples (Fig. 16A). The stable/unstable heavy minerals versus garnet/epidote ratios of the Kharga sand sediments and their proposed sources are given in Fig. 16B. The Kharga dune samples are enriched in stable minerals, and they are plotted in an area close to samples of late Pleistocene dune sand and Holocene playa sand. They are also plotted in a field nearer to the Moghra sandstone than the Nubian sand field. This also indicates that the source of the Kharga aeolian sand is mainly Moghra sandstone with contributions from ancient dune and alluvial sands.

History of Kharga barchan sands

The history of the aeolian sand includes three stages (Aufrére (1934): (1) formation of sedimentary basin; (2) transportation and accumulation of alluvial deposits, and (3) formation of dune sands by reworking of the alluvial deposits by wind action. Accordingly, most authors agree that alluvial fans of large endorheic stream systems are a source of aeolian sands (Besler 2008). In the case of Abu Muharak dunes (Fig. 17), the sedimentary basin was formed by tectonic and climatic conditions since the Late Eocene, when the Mediterranean Sea retreated northward, and the Red Sea rift emerged in Oligo-Miocene time (Hamdan and Hassan 2020). Consequently, there was major uplift in Eastern Egypt and huge Red Sea mountains and plateaus were formed on several pulses. During Tertiary, Egypt has drained several major drainage systems, (Issawi and McCauley 1993; Ghoneim and El-Baz 2007). Among these rivers, the Gilf system (c. 40 to 24 million years) consisted of rivers that formed on the flanks of the Red Sea region and extended in a northwest direction. The deposits of these rivers are represented by the deltaic and alluvial deposits in northern Egypt at Siwa, Qattara (Moghra sandstone), and Faiyum (Qattrani and Gebel El Khasab formations) as well as alluvial deposits exposed in different parts of the Western Desert, e.g., Radar rivers and inverted wadis (McCauley et al. 1982, 1986). The abovementioned alluvial stages are inherited in the mineralogy and surface features of the modern barchan sands by the abundance of conchoidal fractures in the aeolian grains (Fig. 17).

The advent of early Pleistocene arid conditions led to the deflation of the sediments of the Radar River into a vast flat sand sheet in southwest Egypt and northwest Sudan (Maxwell and Haynes 2001). The middle Pleistocene humid condition leads to the formation of the alluvial deposits (inverted Wadis; Giegengack and Zaki 2017) and the formation of huge playa lakes (Middle Paleolithic playa; Hamdan and Hassan 2020) on the depressions previously formed by the abovementioned rivers. During late Pleistocene hyperarid conditions, at least two generations of aeolian sand accumulation were recorded in the Western Desert (i.e., 65 to 20 ka and 13,000 BP). The abundance of intensive chemical weathering surface features and conchoidal fractures in the grains of the Kharga barchan sands reflect the complex alluviation history of the Western Desert of Egypt (see Fig. 9; Fig. 17).

Under the early Holocene (11 – 7 ka BP) humid climate, the late Pleistocene dunes were stabilized as indicated by the existence of paleosol and vegetation remains (Besler 1998). Moreover, the surface slope sediments of the weathered Nubian sandstone were reworked into playa lakes and alluvial channels. During that time, a branch of the river Nile passed through the Kharga Depression and deposited channel and flood plain sediments (El-Baz 1998). The lacustrine playa environment is reflected in the surface of the Kharga barchan sand as reddening and clay coating (see Fig. 9). The late Holocene arid and hyper-arid climate in the Western Desert of Egypt started c. 4500 BP (Kuper 2006) and led to the formation of the modern active dune sand in the whole Western Desert including the Kharga Depression. The major parts of the Abu Muharak dune belt were derived from Moghra Formation in the northern Depression, e.g., Qattara with contributions from local sources such as alluvial and ancient dunes as well as weathered Nubian sandstone. These contributions are evidenced by (a) the increase in mean grain size and percentages of angular grains, probably inherited from contribution from Holocene alluvial sediments; (b) the increase in proportions of the stable mineral quartz, especially single grains with unit extinction; accompanied by a decrease in those of the less stable minerals; and (c) the nature and distribution of the heavy-mineral assemblage present which shows a marked abundance of stable heavy minerals with some pyroxene, which contributed from the Holocene Nile sediment terraces in Kharga barchan sands.

Conclusions

The grain size, roundness, sphericity, and surface features of the barchan sands were studied. The mean of Kharga barchan sands varies between 1.61 to 2.51 Φ with an average value of 2.11 Φ and the sands of the crest and mid-slip are always finer and better sorted than other barchan sands. The Kharga barchan sands are characterized by round to subrounded, and spherical grains. Little differences were noticed in the roundness characteristics between the sands of the different dune types of the same size. Nevertheless, there is a significant variation in the roundness parameters of the size fraction; the mean roundness value decreases with the decrease in grain size, i.e., the roundness characteristics of the Kharga sands are controlled to a great extent by their grain size. SEM examination of the barchan sands exhibits surface features that are related to mechanical and chemical processes that are mostly inherited from the previous paleoenvironments of the source sands.

There is a little variation in the sand's texture, mineralogy, and geochemistry from north to south of the Kharga dune field. The mean size of the barchan sands is a little coarse, with worse sorting and strong positive skewed in the central and southern parts of the dune field. The roundness and sphericity of the barchan sands of the northern part of the dune field are much better than those of the southern portion. The sands of the central and southern portions of the Kharga dune field are enriched in metamorphic mineral grains than the other parts. The Kharga dune field is geochemically homogeneous except for some samples which have a higher percent of CaO and Al_2O_3 referring to contribution from local limestone and shale, respectively.

Textural, mineralogical, and chemical proxies of the Kharga dunes indicate that the Lower Miocene Moghra sandstone is the main provenance of the Abu Muharak dune belt with a contribution of local sources such as alluvial deposits, ancient dunes, and weathered Nubian sandstone, particularly in the Kharga Depression. Sands were derived mainly from older (late Pleistocene) dune sand to the north of the study area. The older dune sands were previously sourced from the Nubian sandstone through the complex history of alluviation and wind deflation corresponding to alternating humid and arid climatic conditions since the late Tertiary. Contribution from local sources in the Kharga Depression added several textural and mineralogical elements.

Acknowledgements The field and laboratory were funded by the Geology Department, Faculty of Science, Cairo University, to the first author (S. Ramadan) as part of his Master's thesis. Textural and heavy mineral analyses were carried out in the sedimentology laboratory of the Geology Department at Cairo University.

Funding Open access funding provided by The Science, Technology & Innovation Funding Authority (STDF) in cooperation with The Egyptian Knowledge Bank (EKB).

Declarations

Conflict of interest The authors declare that they have no competing interests.

References

Ahlbrandt TS (1979) Textural parameters of aeolian deposits. In: McKee ED (ed) A study of global sand seas. US Geological Survey Professional Paper 1052, Washington, pp 21–51

Aufrére L (1934) Les dunes du Sahara alge´rien. Bulletin de 1`Association de Ge´ographes Franc¸ais 83:130–142
Bagnold RA (1941) The physics of the blown sand and desert dunes. Chapman and hall, London
Ball J (1927) Problems of the Libyan Desert. Geogr J 70:21-28, 105-129, 209-225
Barrett PJ (1980) The shape of rock particles, a critical review. Sedimentology 27:291–303
Beadnell L (1910) The sand dunes of the Libyan Desert. Geogr J 35:379–395
Besler H (1980) Die Du¨nen-Namib: Entstehung und Dynamik eines Ergs. Stuttgarter Geographische Studien 96, 241 pp
Besler H (1986) The Toshka-Canal dune: analysis of development and dynamics. ln: Nickling WG (ed) Aeolian geomorphology. The Binghamton Symposia in Geomorphology. International Series 17, Allen & Unwin, Boston, pp 113–130
Besler H (1998) Periods of aeolian activity and stability in the Great Sand Sea in Egypt. Zbl Geol Paläontol 1(1997):23–39
Besler H (2000) Modern and Paleo-modeling in the Great Sand Sea of Egypt (initial results from the Cologne Cooperative Research Project 389). In: Kröpelin S, Petit-Maire N (eds) Palaeomonsoon variations and global change during the Late Quaternary. Global and Planetary Change 26, Elsevier, Amsterdam, pp 13–24
Besler H (2008) The Great Sand Sea in Egypt. Developments in Sedimentology 59, Elsevier Publ., Amsterdam
Blatt H, Christie JM (1963) Undulatory extinction in quartz of igneous and metamorphic rocks and its significance in provenance studies of sedimentary rocks. J Sediment Petrol 33:559–579
Campbell DH (1963) Percussion marks on quartz grains. J Sediment Res 33:855–859
Conoco Coral (1987) Geological map of Egypt, Scale 1:500,000, Egyptian General Petroleum Corporation-Conoco Coral, Cairo. Sheet NG 36 NW Asyut
El-Baz F (1988) Origin and evolution of the desert. Interdiscip Sci Rev 13:331–347
El-Baz F (1998) Aeolian deposits and palaeo-rivers of the eastern Sahara. Significance to archaeology and groundwater exploration. Sahara 10:55–66
El-Baz F, Wolfe RW (1982) Wind patterns in the Western Desert. In: El-Baz F, Maxwell TA (eds) Desert landforms of southeast Egypt: a basis for comparison with Mars. NASA CR-3611, pp 119–139
El-Baz F, Slezak MH, Maxwell TA (1979) Preliminary analysis of color variations of sand deposits in the Western Desert of Egypt. In: El-Baz F, Warner DM (eds) Apollo-Souez Test Project- Earth observations and photography. NASA, Washington, D.C., pp 237–262
El Gammal EA, Cherif OH (2006) Use of remote sensing for the study of the hazards of Ghard Abu Muharik sand dune field, Western Desert, Egypt. The 2nd International Conf. on Water Resources and Arid Environment. NARS, Cairo, pp 1–20
Embabi NS (1982) Barchans of the Kharga depression. In: El-Baz F, Maxwell TA (eds) Desert landforms of southwest Egypt: a basis for comparison with Mars. NASA. (CR-3611), Washington, DC, pp 141–155
Embabi NS (2017) Landscapes and landforms of Egypt: landforms and evolution. World Geomorphological Landscapes, 336 pp. https://doi.org/10.1007/978-3-319-65661-8
Embabi NS, Mostafa AA, Mahmoud AA, Azab MA (2012) Geomorphology of Ghard Abu Muharak Sand Sea. Egypt Bull Soc Géogr D'Égypte 58:1–28
Folk RL (1955) Student operator error in the determination of roundness, sphericity, and grain size. J Sediment Petrol 25(4):297–301
Folk RL (1969) Grain shape and diagenesis in Simpson Desert, Northern territory, Australia. Geol. Soc. America Abstract, 68–69
Folk RL (1971) Longitudinal dunes of the northwestern edge of the Simpson Desert, Northern Territory, Australia. 1. Geomorphology and grain size relationships. Sedimentology 16:5–54
Folk RL (1978) Angularity and silica coatings of Simpson Desert sand grains, Northern territory, Australia. J Sed Petrol 48:611–624
Folk RL, Ward WL (1957) Brazos River bar, a study in the significance of grain parameters. J Sediment Petrol 27:3–27
Giegengack R, Zaki A (2017) Inverted topographic features, now submerged beneath the water of Lake Nasser, document a morphostratigraphic sequence of high amplitude late-Pleistocene climate oscillation in Egyptian Nubia. J Afr Earth Sci 136:176–187
Gifford AW, Warner DM, El-Baz F (1979) Orbital observation of sand distribution in the Western Desert of Egypt. In: El-Baz F, Warner D (eds) Apollo-Soyuz Test Project summary science report, vol II. National Aeronautics and Space Administration, Washington DC
Ghoneim E, El-Baz F (2007) The application of radar topographic data to mapping of mega-paleodrainage in the Eastern Sahara. J Arid Environ 69:658–675
Goudie AS, Watson A (1981) The shape of desert sand dune grains. J Arid Environ 4:185–190
Goudie AS, Allchin B, Hegde KTM (1973) The former extensions of the great Indian sand desert. Geogr J 139:243–257
Goudie A, Warren A, Jones D, Cooke R (1987) The character and possible origins of the aeolian sediments of the Wahiba sand sea, Oman. Geogr J 154:231–256
Griffiths JC (1967) Scientific method in analysis of sediments. McGraw-Hill, New York, p 508
Hamdan MA (1987) Geomorphology and Quaternary Geology of Umm El Dabadib area Kharga Oasis, Western Desert Egypt. M. Sc. Thesis, Fac. of Science, Cairo University
Hamdan MA (2003) Textural, mineralogical, and geochemical characteristics of the aeolian dune sand of the Gilf-Uwinat area, south Western Desert. 5th International conf. of the geology of the Middle East, pp 171–187
Hamdan MA, Refaat AA (1999) Textural and mineralogical characteristics and distributions of aeolian sand deposits at Qattara-Siwa area, northwestern desert, Egypt. Int. Conf. on Geol. of the Arab World, GAW4, 1998, Cairo Univ., Egypt, pp 684–706
Hamdan MA, Hassan FA (2020) Quaternary of Egypt. In Hamimi Z, El Barkooky A, Frias JM, Fritz H, Abd El-Rahman Y (eds) The geology Of Egypt. Springer Nature Switzerland AG, pp 455–494
Hassan S, Steel R, El Barkooky A, Hamdan M, Olariu C, Helper M (2012) Stacked Lower Miocene tide-dominated estuary deposits in a transgressive succession, Western Desert, Egypt. Sediment Geol 282:241–255
Hamdan MA, Refaat AA, Abu Anwar E, Shallaly NA (2015) Source of the aeolian dune sand of Toshka area, southeastern Western Desert, Egypt. Aeolian Res 17:275–289
Hamdan MA, Refaat AA, Abdel WM (2016) Morphologic characteristics and migration rate assessment of barchans dunes in the Southeastern Western Desert of Egypt. Geomorphology 257:57–74
Hamdan MA, Hassan FA, Flower RJ, Leroy SAG, Shallaly NA, Flynn A (2019) Source of Nile sediments in the floodplain at Saqqara inferred from mineralogical, geochemical, and pollen data, and their palaeoclimatic and geoarchaeological significance. Quat Int 501:272–288
Issawi B, McCauley J (1993) The Cenozoic landscape of Egypt and its river systems. Ann Geol Surv Egypt 19:357–384
Kasper-Zubillaga JJ (2009) Roundness in quartz grains from inland and coastal dune sands, Altar Desert, Sonora, Mexico. Bol Soc Geol Mex 61:1–12
Khalaf FI, Gharib IM (1985) Roundness parameters of quartz sand grains of recent aeolian sand deposit in Kuwait. Sediment Geol 45:137–158
Krinsley DH, Doornkamp JC (1973) Atlas of quartz sand surface textures. University Press, Cambridge, p 91

Krumbein W (1941) Measurement and geological significance of shape and roundness of sedimentary particles. J Sediment Petrol 11:64–72
Kuenen PhH (1960) Experimental abrasion for aeolian action. J Geol 68:427–449
Kukal Z (1971) Geology of recent sediments: London. Academic Press, New York, p 490
Kuper R (2006) After 5000 BC: The Libyan Desert in transition. C R Palevol 5:409–419
Lancaster N (1981) Paleoenvironmental implications of fixed dune systems in Southern Africa. Palaeogeogr Palaeoclimatol Palaeoecol 33:327–346
Lancaster N (1986) Grain-size characteristics of linear dunes in the southwestern Kalahari. J Sediment Petrol 56:395–400
Lancaster N (1995) Geomorphology of desert dunes. Routledge, London, New York
Le Ribault L (1977) L' exoscopie des Quartz. Masson, Paris, p 150p
MacCarthy GR (1935) Eolian sands: a comparison. Am J Sci 5th set. 176(30):81–95
MacCarthy GR, Huddle JV (1938) Shape sorting of sand grains by wind action. Am J Sci 5th set 35(205):64–73
Mahaney WC (2002) Atlas of sand grain surface textures and applications. University Press, Oxford, p 237
Mason CC, Folk RL (1958) Differentiation of beach, dune, and aeolian flat environments by size analysis, Mustang Island, Texas. J Sediment Petrol 28:211–226
Mattox RB (1955) Eolian shape-sorting. J Sediment Petrol 25:111–114
Maxwell TA (1982) Sand sheet and lag deposits in the southwestern desert. In: El-Baz F, Maxwell TA(eds) Desert Landforms of Southwest Egypt: A Basis for Comparison with Mars. NASA Cr-3611, pp 157–173
Maxwell TA, Haynes CV (2001) Sand sheet dynamics and Quaternary landscape evolution of Selima Sand Sheet, southern Egypt. Quat Sci Rev 20:1623–1647
Mazzullo J, Sims D, Cunningham D (1986) The effects of eolian sorting and abrasion upon the shapes of fine quartz sand grains. J Sediment Petrol 56:45–56
McCauley JF, Schaber GG, Breed CS, Grolier MJ, Haynes CV, Issawi B, Elachi C, Blom R (1982) Subsurface valleys and geoarchaeology of the eastern Sahara revealed by Shuttle radar. Science 218:1004–1020
McCauley JF, Breed CS, Schaber GG, McHugh WP, Issawi B, Haynes CV, Grolier MJ, El Kilani A (1986) Paleodrainages of the Eastern Sahara – the radar rivers revisited (SIR - A/B implications for a mid-Tertiary Trans-African Drainage system). IEEE Trans Geosci Remote Sens GE-24:624–648
McLaren P (1981) An interpretation of trends in grain size measures. J Sediment Res 51:611–624
Milner HB (1962) Sedimentary petrography. George Alien & Unwin., Ltd., London, vol 1, p 643; vol 2, p 715
Norris RM, Norris KS (1961) Algodones dunes of southeastern California. Geol Soc Am Bull 72:605–620
Pandey S, Singh S, Ghose B (1971) Orientation, distribution, and origin of sand dunes in the central Luni begin. Proc. Symp. Problems of Indian Arid zone, Jodhpur, pp 94–91
Pettijohn FJ (1957) Sedimentary Rocks, 2nd edn. Harper, New York, p 718
Powers MC (1953) A new roundness scale for sedimentary particles. J Sediment Petrol 23:117–119
Pye K (1982) Negatively skewed aeolian sands from a humid tropical coastal dune field, Northern Australia. Sediment Geol 31:249–266
Pye K, Tsoar H (2009) Aeolian sand and sand dunes. Springer-Verlag, Berlin Heidelberg, p 456p
Refaat AA, Hamdan MA (2015) Mineralogy and grain morphology of the aeolian dune sand of Toshka area, southeastern Western Desert, Egypt. Aeolian Res 17(2015):243–254
Richardson H (1903) Sea sand. Annu. Rep. Yorks. Philos Soc 1902:43–58
Roskin J, Katra I, Blumberg DG (2014) Particle-size fractionation of eolian sand along the Sinai-Negev erg of Egypt and Israel. Geol Soc Am Bull 126(1–2):47–65
Said R (1962) The geology of Egypt. Elsevier, Amsterdam, p 377
Said R (1998) Sand accumulation and groundwater in the eastern Sahara: a rebuttal to El-Baz, F. Episodes 21(3):287–289
Sharaky AM (1990) Geomorphological studies on sand dunes and ridges in some African deserts. M.Sc. thesis, Institute of African Research and studies, Cairo University
Shepard FP, Young R (1961) Distinguishing between beach and dune sands. J Sediment Petrol 31(2):196–214
Shukri NM (1950a) The mineralogy of some Nile sediments. Q J Geol Soc Lond 105:511–534
Shukri NM (1950b) The mineralogy of some Nile sediments. Q J Geol Soc Lond 105:511–534
Shukri NM, Ayouty MK (1953) The mineralogy of Nubian sandstone in Aswan. Bull Inst Desert D, Egypte 3:65–88
Thomas DSG (1984) Ancient ergs of the former arid zones of Zimbabwe, Zambia and Angola. Transactions, Institute of British Geographers, NS, 9, 75–88
Tsoar H (1978) The dynamics of longitudinal dunes: final technical report. US Army European Research Office (171 pp)
Turekian KK, Wedepohl KH (1961) Distribution of the elements in some major units of the Earth's crust. Geol Soc Am Bull 72:175–192
Visher GS (1969) Grain-size distributional processes. J Sediment Petrol 39:1074–1106
Wasson RJ (1983) Dune sediment types, sand colour, sediment provenance and hydrology in the Strzelecki-Simpson Desert, Australia. In: Brookfield ME, Ahlbrandt TS (eds) Eolian Sediments and Processes. Elsevier, Amsterdam, pp 165–196
Woronko B, Dłużewskib M, Woronko D (2017) Sand-grain micromorphology is used as a sediment-source indicator for Kharga Depression dunes (Western Desert, S Egypt). Aeolian Res 29:42–54
Zhu B (2007) Geochemistry, hydrochemistry and sedimentology of the Taklamakan Desert in Tarim Basin, NW China. (Ph.D Thesis) Institute of Geology and Geophysics Chinese Academy of Sciences (IGGCAS), Beijing, China
Zhu B-J, Yu J, Rioual P, Ren X (2014) Particle size variation of aeolian dune deposits in the lower reaches of the Heihe River basin, China. Sed Geol 301:54–69